

POLITECNICO DI TORINO

**Master of Science
in Mechanical Engineering**

Master's Thesis

Multi jet Fusion and Selective Laser Sintering: a 3D printing technology comparison



Supervisors

Prof. Luca Iuliano
Prof. Flaviana Calignano

Company Supervisor

Eng. Roberta Sampieri

Candidate

Ehsan Lesani

Academic Year 2019-2020

CONTENTS

I.	Summary.....	5
I.I	Introduction	5
I.II	Objectives	6
I.III	Main Results	6
I.IV	Abstract	7
1.	Introduction to Additive Manufacturing	8
1.1.	Additive Manufacturing technology	8
1.2.	Powder Bed Fusion	12
1.3.	SLS – Selective Laser Sintering	14
1.4.	Multi Jet Fusion – HP 3D printing technology	21
2.	Experimental Analysis	30
2.1.	The SLS Machine	30
2.2.	The MJF Machine	32
2.3.	The AM Material PA 12	40
3.	Testing information and standards.....	44
3.1.	The Tensile Test	44
3.2.	The Standards	49
4.	Results.....	52
4.1.	Output data of the Tensile Testing Machine	52
4.2.	Results for Multi Jet Fusion technology	57
4.3.	Results for SLS technology	61
4.4.	Overall comparison charts, MJF vs SLS	65
5.	Conclusions	68
A.	List of Tables	70

B. List of Figures	71
C. Abbreviations	73
D. Bibliography	74
E. Acknowledgments	77

I. Summary

I.I Introduction

Additive manufacturing, or 3D printing, is the construction of a three-dimensional object from a CAD model or a digital 3D model [1]. The term "3D printing" can refer to a variety of processes in which material is joined or solidified under computer control to create a three-dimensional object [2], with the material being added together (such as liquid molecules or powder grains being fused), typically layer by layer.

In the 1990s, 3D printing techniques were considered suitable only to produce functional or aesthetic prototypes, and a more appropriate term for it at the time was rapid prototyping [3]. As of 2019, the precision, repeatability, and material range of 3D printing has increased to the point that some 3D printing processes are considered viable as an industrial-production technology, whereby the term additive manufacturing can be used synonymously with 3D printing. One of the key advantages of 3D printing is the ability to produce very complex shapes or geometries that would be otherwise impossible to construct by hand, including hollow parts or parts with internal truss structures to reduce weight [4].

In this study, two states of the art Powder Bed Fusion (PBF) additive manufacturing technologies, Multi Jet Fusion and Selective Laser Sintering, are compared, mainly in their mechanical properties of the produced final parts. The thesis is carried out in collaboration with the Fiat Chrysler Automobiles EMEA PD Additive Manufacturing Centre and the Integrated Additive Manufacturing (IAM@PoliTO) Center of Politecnico di Torino.

I.II Objectives

The two technologies studied in this thesis have many differences in the process flow, the processing time, etc. However, the main focus of this thesis was on the mechanical properties of the final products. In additive manufacturing, which is a method of production layer by layer, the mechanical properties are assumed to vary in different orientations. In this thesis, nine different orientations are considered for the production of the specimens by each technology, and these specimens are used in tensile tests to obtain the experimental values of the mechanical properties. The tensile test provides a lot of information regarding the mechanical properties such as ultimate tensile strength, the elastic modulus, the elongation at break, etc. These mechanical properties are crucial for predicting the behavior of the final product in the designed applications.

I.III Main Results

Regarding the results obtained after 90 tensile tests carried out on the specimens for the two technologies, some similarities and some differences are noticeable in the comparison charts reported for each mechanical property in this study. According to the results, the main differences are related to the Elastic Modulus values, which for the SLS specimens, they are much higher than the values for the MJF specimens, and the Elongation at Break percentage, in which the SLS specimens show much more different behavior in different orientations of the production. This is very important in the part design process, since in this case for example the specimen produced in any of the Z-axis directions (ZD, ZX, and ZY) cannot be used in the condition which requires a fair amount of deformability. In this case, the material will show a sudden brittle fracture.

I.IV Abstract

This work aims to compare the two state of the art Powder Bed Fusion Technologies, mainly from the mechanical properties point of view. For making a good comparison of the two technologies, five stages have been followed in this thesis.

In the first stage, an adequate standard for the tensile test, and for the specimen used had to be chosen. This stage is very important because the chosen standard can affect the values of some of the results, and by considering a standard which is not used by the other institutes or laboratories, the value of the work and results will decrease, since they cannot be compared to the results of the other works related to these technologies.

In the second stage, the specimen had to be designed according to the standard. Nine different printing orientations had been chosen, and consequently, a specific name was given to each of the designed specimens for each of the printing orientation.

The third stage consists of preparing the job in the HP Jet Fusion 4200 and the SLS 3d printer FORMIGA P 110, and finally printing the 45 specimens in 9 different orientations for each of the two technologies. After the cleaning process, the parts were ready for the tensile tests.

In the fourth stage, all the specimens had to undergo a tensile test. With the help of MATLAB and the Force-Elongation data received from the tensile testing machine, the final stress-strain curves were obtained.

In the fifth and final stage, after reporting the values of each mechanical properties in the comparison bar charts, comparing the values and obtaining the final results were done with a lot of care and attention.

It has to be mentioned that this work was a collaboration of the Fiat Chrysler Automobiles EMEA PD Additive Manufacturing Centre with Politecnico di Torino Integrated Additive Manufacturing (IAM@PoliTO) Center, and the parameters used in the production phase of the specimens, such as the mixed powder ratio, the printing speed, etc., were the ones used in the real industrial condition, and not necessarily the same as the parameters used by the manufacturers of the powders and the machines to obtain the datasheets of their products.

1. Introduction to Additive Manufacturing

1.1. Additive Manufacturing technology

The term “additive manufacturing (AM)” references technologies that grow three-dimensional objects one superfine layer at a time. Each successive layer bonds to the preceding layer of melted or partially melted material. It is possible to use different substances for layering material, including metal powder, thermoplastics, ceramics, composites, glass, and even edibles like chocolate [5].

Objects are digitally defined by computer-aided-design (CAD) software that is used to create .stl files that essentially "slice" the object into ultra-thin layers. This information guides the path of a nozzle or print head as it precisely deposits material upon the preceding layer, or a laser or electron beam selectively melts or partially melts in a bed of powdered material. As materials cool or are cured, they fuse to form a three-dimensional object [5].

Although the terms "3D printing" and "rapid prototyping" are casually used to discuss additive manufacturing, each process is a subset of additive manufacturing [5].

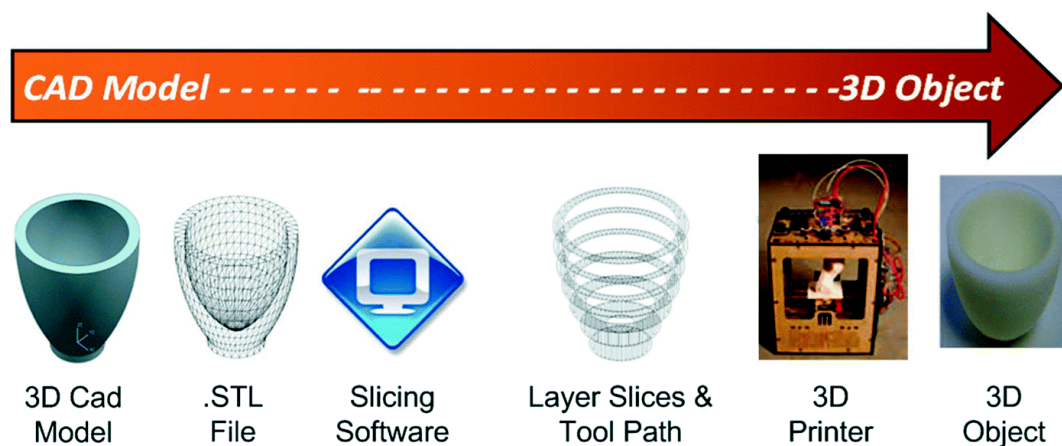


Figure 1.1 – The 3d printing technology schematic steps [6]

AM technologies have expanded vastly over more than 20 years of its history (beginning with the initial commercialization of stereolithography in 1987). Originally seen as most suitable for rapid prototyping (RP), these processes are no longer exclusively used for that purpose. With the advent of new materials along with new processes, each technology has been contributing to the diversities in different fields of application [7] (see figure 1.2).

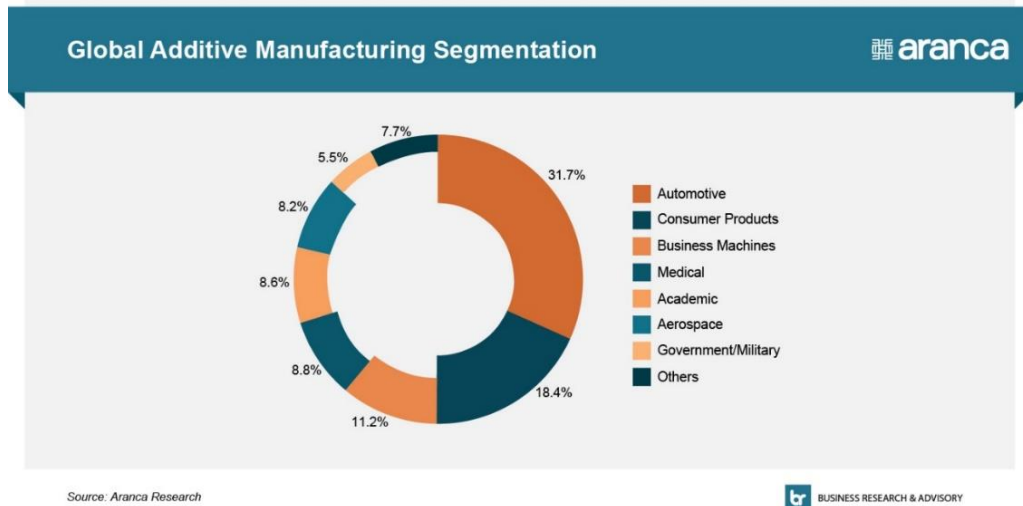


Figure 1.2 – Global Additive Manufacturing segmentation [8]

The emergence of 3D-printed components has generated significant new opportunities in the aerospace, automotive, medical devices, and tooling industries to name a few [9].

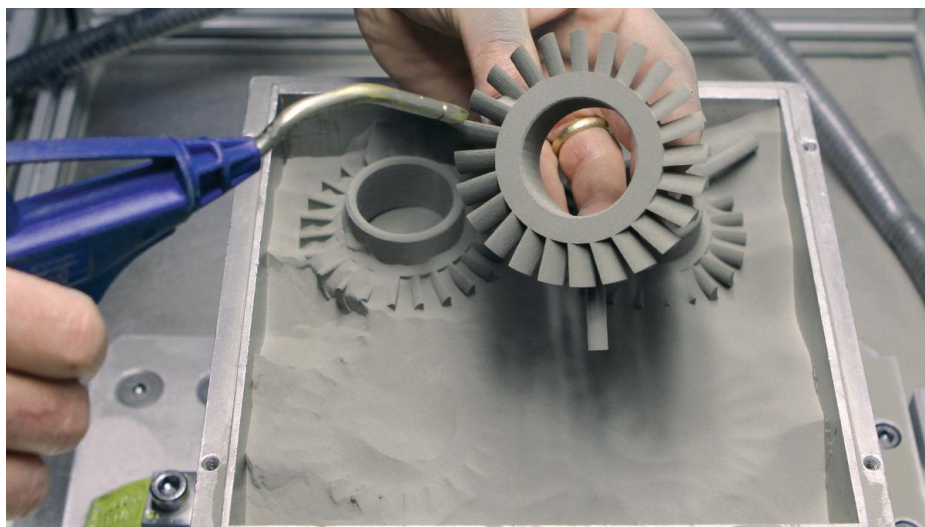


Figure 1.3 – Using Additive Manufacturing parts in the industries [10]

During the last 20 years, intensive research efforts have been focused primarily on the so-called high-end additive processes and above all on stereolithography (SLA) and selective laser sintering/selective laser melting (SLS/SLM) technologies, exploring various issues mostly related to process control and material property improvement [7].

In recent years, three-dimensional printing (3DP) came to the foreground as a very competitive process in terms of cost and speed [7]. Additive Manufacturing market size is anticipated to grow even more during the coming years (figure 1.4).

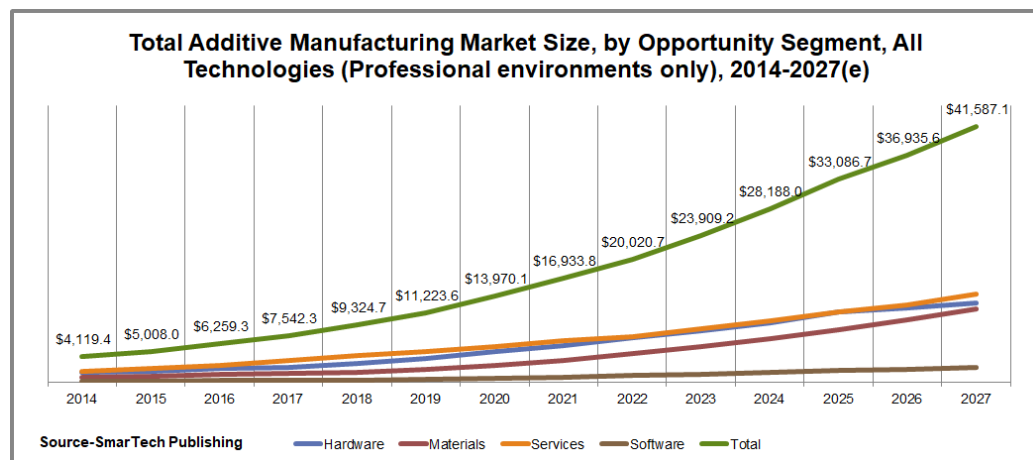
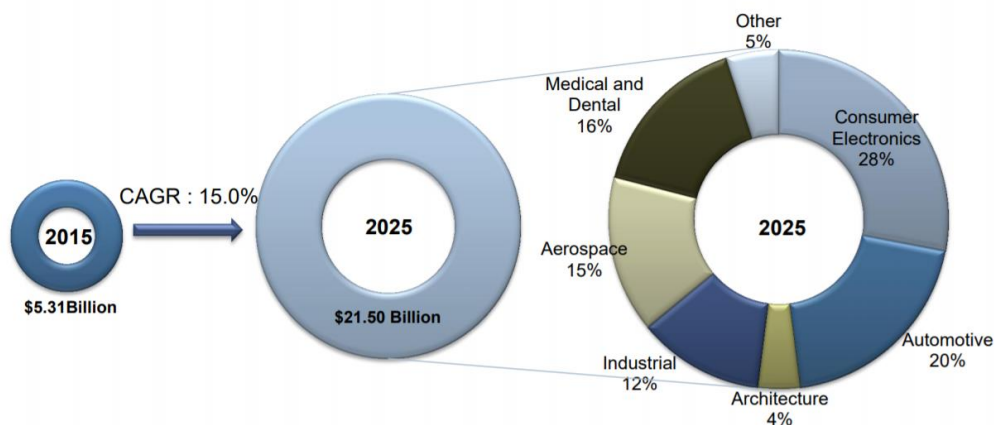


Figure 1.4 – The Additive Manufacturing Market size anticipation [11]

From a study in 2016 by Frost & Sullivan's Global 360° Research Team, the market of additive manufacturing will face considerable growth until 2025 [12] (see figure 1.5).



Others include Energy, Construction, Food & Beverage, and others

Source: Frost & Sullivan

Figure 1.5 – The revenue generation anticipation for the future of Additive manufacturing (2015-2025) [12]

Since its announcement, a large variety of 3DP techniques have been introduced into the AM industry. All these techniques have their roots in inkjet printing technology, and the use of a printer head is the only element they have in common. This printer head – in whatever version it might be applied – serves to shoot either droplet of binder or liquid-to-solid compound, and so it forms a layer of an object model. The shooting of droplets of the actual building material (liquid-to-solid compound) in DoD mode is known as a drop-on-drop deposition, while the shooting of droplets of binder on the powder material is called drop-on-powder (DoP), or drop-on-bed (DoB) deposition [7].

With the larger selection of materials available today, as well as the wide variety of post-treatment procedures, the scope for Additive Manufacturing technology is growing quickly, far beyond the original idea of generating design iterations or inexpensive metal parts directly from a computer-aided design (CAD) file [7].

1.2. Powder Bed Fusion

Powder bed fusion (PBF) is a subset of additive manufacturing (AM) whereby a heat source (eg, laser, thermal print head) is used to consolidate material in powder form to form three-dimensional (3D) objects. The heat source is applied to particles contained within a powder bed, which gradually indexes down as each layer is completed and new powder is spread over the build area. Powder Bed Fusion techniques share the basic principles of all AM techniques (eg, layer-by-layer fabrication directly from 3D model data) as well as common advantages such as cost-effective customization and reduced assembly [13].

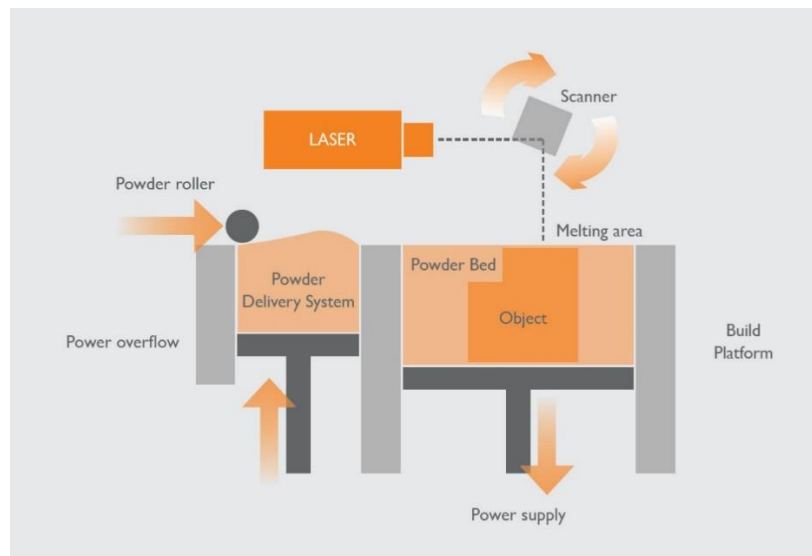


Figure 1.6 – Schematic of the printing process for a PBF technology (SLS in this case) [14]

Polymer PBF processes have a significant advantage over many other AM processes in that they do not require support structures since overhangs and unconnected islands are supported by the surrounding unfused powder bed (see figure 1.7). This allows more complex geometries to be produced, as removal of support structures after the build does not need to be considered [13].

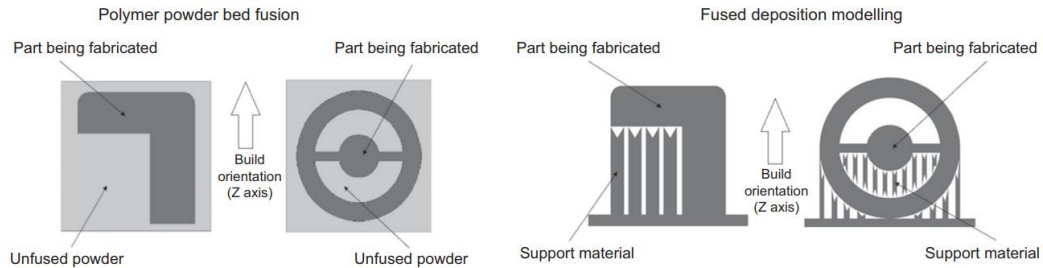


Figure 1.7 – Schematic illustrating the ability of polymer powder bed fusion to produce parts with overhangs and unsupported islands without support structures (left) compared with other AM processes, for example, fused deposition modeling (right), in which these structures must be supported during the build process [13].

The lack of support structures also means that parts can be stacked freely in the powder bed, increasing the number of parts that can be produced in each build and thus increasing productivity (see figure 1.8). However, there are some design limitations in terms of the removal of unfused powder from trapped volumes (eg, enclosed pores) and fine channels. Another advantage of PBF techniques is the wide range of materials that can potentially be processed: Any material that can be melted and resolidified can, in theory, be used with PBF techniques [13].

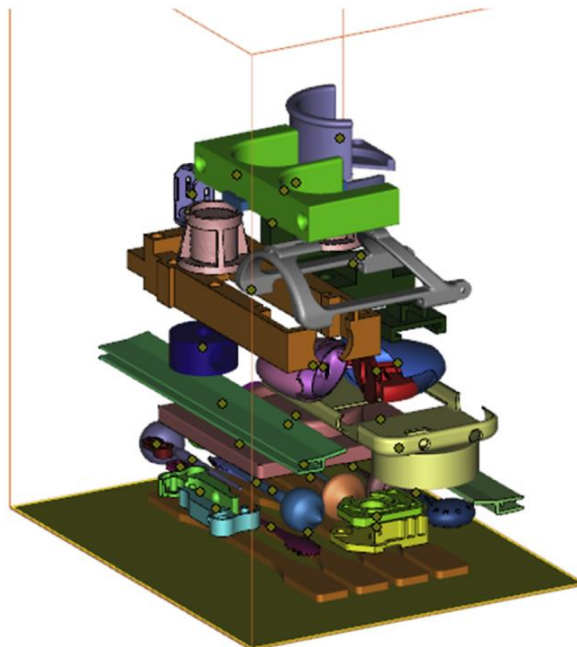


Figure 1.8 – A typical laser sintering build set-up consisting of multiple individual parts. Because no support structures are required, parts can be placed freely in the entire build volume without being connected to the part below [13].

Table 1.1 shows the classification of Powder bed fusion technologies. The thesis aims to make a comparison of the first two technologies from the top, Multi Jet Fusion (MJF) and Selective Laser Sintering (SLS).

Powder bed fusion	Multi-Jet Fusion (MJF)	Fused with agent and energy
	Selective laser sintering (SLS)	Fused with laser
	Direct Metal Laser Sintering (DMLS)/Selective Laser Melting (SLM)	Fused with laser
	Electron Beam Melting (EBM)	Fused with electron beam

Table 1.1 – Classification of Powder bed fusion/additive manufacturing technology [15]

1.3. SLS – Selective Laser Sintering

Laser sintering is one of the most common and widely accepted AM processes. It produces parts by selectively fusing individual layers of powdered material using a laser (typically a carbon dioxide laser) [13].

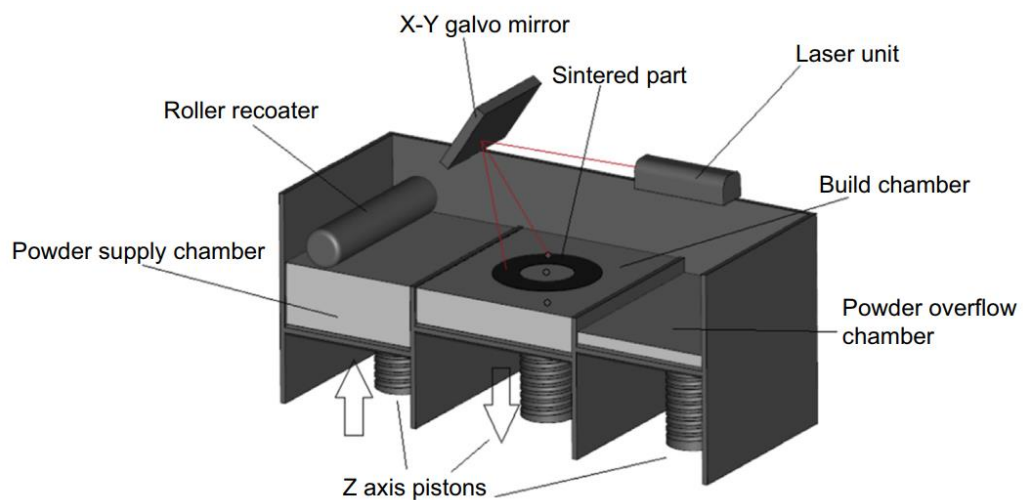


Figure 1.9 – Schematic of a simplified laser sintering technology [13]

An STL file of the part to be fabricated is sliced into cross-sectional layers. A layer with a thickness of 100 to 150 μm is commonly used. The powder is spread over the build platform and leveled using a roller, recoating blade, or alternative device [13]. Before commencing fabrication of a part or series of parts, the powder bed is normally heated gradually from room temperature to the desired processing bed temperature, typically throughout 1 to 2 h, depending on the final temperature to be reached [13]. This is known as the ‘warm-up’ phase. The powder bed continues to be heated during the processing phase. Processing begins with the build platform, which is moveable in the z-direction, indexing down by one-layer thickness and the spreading of a thin layer of powder over the build area. Selected regions of this powder layer are fused by the laser according to the cross-sectional data from the STL file. The platform is lowered, and a fresh layer of powder is spread over the previously scanned layer [13]. A scan corresponding to the next cross-sectional layer of the part causes powder particles to fuse within that layer and to the underlying layer, where required. These processing steps are repeated until the 3D part is completed [13]. During part production, laser sintering does not require structures to support overhangs because the un-melted powder within the powder bed supports the melted polymer [13]. Upon completion of the parts, the powder bed and the parts contained within it (often referred to as the ‘part cake’) are allowed to cool down before being removed from the build chamber [13]. The un-sintered powder can be reused to a certain extent depending on the type of polymer [13]. The manufactured parts can now be used or refined in conformance with their proposed application [13].

A few different process parameters can be modified, including laser parameters (e.g. laser power and scan speed) and build parameters (eg, layer thickness) [13]. The most modified parameters are described in Table 1.2.

Parameter	Description
Laser power	Applied power of the laser as it scans the area of each layer
Scan speed	Velocity at which the laser beam travels as it traverses a scan vector
Scan spacing	Distance between parallel laser scans
Scan count	Number of times the laser beam traverses a scan vector per layer
Scan strategy	Pattern of the laser as it scans over a layer, in combination with the laser parameters used in each specific area
Layer thickness	The distance the build platform lowers for spreading of a new layer of powder
Build temperature	The temperature of the process chamber and/or part bed

Table 1.2 – Laser sintering process parameters [13]

In the laser sintering process, the laser rapidly scans across the powder bed, and the primary fusion of the particles takes place over a short period with no mechanical pressure applied [13]. The part is then cooled slowly, usually over several hours (up to 12 hours); a complex series of events affects the exact cooling rate of each part [13]. The combination of these factors can make consolidation of many polymers challenging. For semi-crystalline materials, the powder bed is typically heated to just below the melting temperature and held at this temperature throughout the process (often referred to as the ‘bed temperature’) [13]. This means that during exposure, the laser is only required to contribute the remaining amount of energy needed to exceed the phase transition and thus selectively melt the material. It also helps to prevent early crystallization of the molten polymer, which could result in localized shrinkage and part distortion [13].

Laser power is one of the main parameters in the process. Its magnitude depends upon the type of materials processed. Polymers could be processed in 5 W while for ceramics, 500 W could be needed. SLS/SLM machines are equipped with a laser of power from 50 to 400 W [16]. The selection of power is not done independently but depends upon other process parameters and spot size. For the same laser power, with a decrease in spot size, higher laser energy density is achieved, which could be used to process higher melting point materials. Laser power also depends upon our aim with powders [16]. If we want to completely melt it, then more power is required [16]. Using higher laser power than required may ablate the metallic powder and degrade the polymer powder so finding a

process window for a given material is important [16]. To carry out process control in the system, laser power has been mostly used as a controlling parameter to cause change into the system online [16]. If the melt pool width changes from the predefined value, laser power is automatically varied (increased or decreased) to control the size of the melt pool. If the aim is to melt the powder partially then less power is required [16]. This gives rise to consistency in mechanical properties and the dimension of the part fabricated by melting powders [16]. However, it is not the laser power alone that creates the size of the melting pools, but this in conjunction with other process parameters such as speed, layer thickness, hatching distance, etc [16].

CO₂, Nd:YAG, and fiber lasers are mostly used in SLS/SLM [16]. Their wavelengths are 10.6, 1.06, and 1.08 μm (from 1.07 to 1.09), respectively. The selection of laser depends upon their power, mode of operation, beam quality, and absorptivity by powders [16]. Polymer and ceramics (oxides) absorb CO₂ much while metals and ceramics (carbides) absorb Nd:YAG more. In other words, a smaller wavelength is absorbed by metals and their alloys while a larger wavelength is absorbed by polymers [16]. Consequently, the machines meant for processing polymers will use CO₂ while for processing metals, Nd:YAG or fiber laser is used. In the case of a mixture of powders, the selection of laser is governed by the type of powder primarily processed [16]. For example, for processing polymer-coated ceramic, where a laser is used to melt polymer to bind ceramics, CO₂ is used [16]. In the case of processing WC–Co mixture, where the laser is used to melt Co to bind rest WC, Nd:YAG or fiber laser is more suitable [16].

Another important parameter to mention is the Scanning strategy, which is a method of scanning a powder bed with a laser beam to increase the fabrication speed and product quality [16]. Good scanning strategy makes the resultant products free from distortion, warp, anisotropy, inaccuracy, and porosity [16]. It generally consists of two types: fill scan and contour scan [16]. Fill scan is used to scan across all areas while a contour scan is used to do scanning at boundaries. A typical example is shown in figure 1.10 where a fill scan is a parallel scan and a contour scan is done by scanning once at boundaries [16]. The first diagram of figure 1.10 shows a parallel scan in one direction while the second diagram shows

a parallel scan with a change in direction at an alternate scan. Scanning time in the first diagram will be more than in the second diagram [16]. It is because, in the first diagram, the laser always starts scanning from the same side, which means the laser has to travel back to the same side after each scan without scanning [16]. This is not the case in the second diagram where the laser can do continuous scanning [16]. Parallel-line scan mode is easy to program/implement and is the most commonly used scan mode in SLS/SLM. These lines could be parallel to the x-axis or y-axis or making some angle (e.g., 45) with these axes [16]. Scanning in a line produces shrinkage stress and anisotropic strength. For making a part in parallel-line scan mode, scanning direction in every successive layer is changed by 90 degrees to decrease the anisotropic buildup [16].

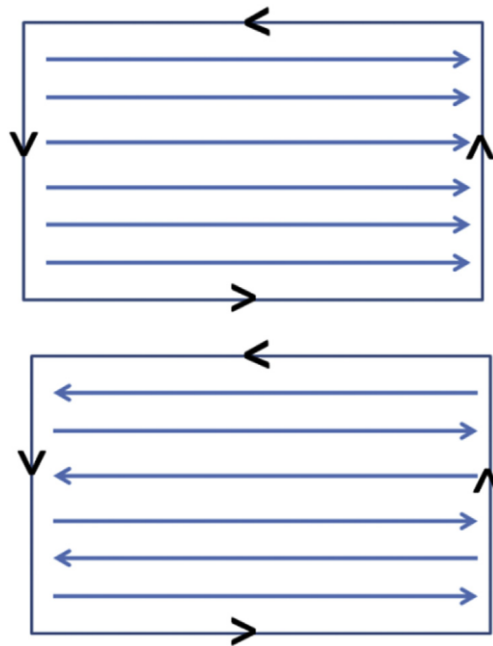


Figure 1.10 – Parallel-line scan mode in the same and alternate directions [16]

The cost of an SLS product depends mainly upon the machine, time, and powder [16]. Since the cost of the machine and powder is high, products are expensive [16]. It is expected that some patents related to system development will expire shortly leading to an increase in the number of system manufacturers. It will decrease the cost of the machine and the product will become relatively cheaper [16].

The development and production of powder are more expensive than the cost of a bigger block of the same material. Powders specially developed for SLS/SLM

process are far more expensive than the general powders [16]. Powders provided by SLS/SLM manufacturers are optimized for a given machine and come up with suggested parameters for processing [16]. The total compositions of these powders are not disclosed, and these are patented powders [16]. It is unlikely that the cost of these dedicated powders will decrease unless there is strong competition from other vendors [16].

EOS SLS Polymer Materials:

At EOS, there are exceptional materials expertise and a comprehensive portfolio of highly developed plastic and polymer materials (3D printing materials) for laser sintering in additive manufacturing [17].

The following 3D printing materials are available for the additive manufacturing of plastic products: polyamides (PA), polystyrenes (PS), thermoplastic elastomers (TPE), polypropylene (PP), and polyaryletherketone (PAEK) [17]. EOS offers a comprehensive selection of materials for the production of plastic parts with additive manufacturing processes. This allows highly customized products to be manufactured in first-class quality [17]. Two of the most common choices among these materials are described in the following.

1. White polyamide 12 powder, also known as nylon, is the most tested material for additive manufacturing on the market. Parts made from nylon are robust, stable for long periods, chemically resistant, and extremely versatile [18]. EOS materials based on polyamide 12 are a high-performance alternative to plastics like ABS or PA6 that have proven their value in injection molding [18]. This cost-efficient general-purpose material is suitable for a variety of applications, including functional prototypes and qualified series production parts from the industry [18]. There are several types of the Polyamide 12 powders produced by EOS, such as PA 2200, PA 2201, PA 2241 FR (Flame-Retardant), PA 2210 FR, PA 3200 GF (Filled With Glass Beads), Alumide® (Filled With Aluminum), PA 640-GSL (Filled With Glass Beads and Carbon Fibers) [18].

Typical mechanical properties	
Tensile modulus	1650 MPa
Tensile strength	48 MPa
Elongation at break	18%
Thermal properties	
Melting temperature (20°C/min)	176°C
Heat deflection temperature (1.80 MPa)	70°C
Heat deflection temperature (0.65 MPa)	154°C
Physical properties	
Density	930 kg/m ³

Table 1.3 – Results for EOS Polyamide 12 (PA 2200) [18]

2. The high-performance plastic polyamide 11 (PA 11) is made from 100% renewable castor beans. PA 11, also known as nylon, is chemically and mechanically heat-resistant and is ideally suited for highly technical applications thanks to its durability [19]. EOS materials of this class are an efficient, impact-resistant alternative to the plastics ABS or PA6, which have proven their value in injection molding. This material is ideally suited for producing functional elements that require high material strength (e.g. living hinges) and/or impact resistance. Therefore, components for which fragmentation is inadmissible (e.g. in the interior of vehicles) are among the typical fields of application [19].

There are several EOS materials of this class, such as PA 1101 (White), PA 1102 (Black), HP 11-30 (High-performance filled With Carbon Fibers), and FR-106 (Flame-Retardant). The results of the mechanical properties and other characteristics for the EOS Polyamide 11 (PA 1102 Black) are reported in the datasheet provided by the producer (see *Table 1.4*).

Typical mechanical properties	
Tensile modulus	1560 MPa XY / 1610 MPa Z
Tensile strength	48 MPa
Elongation at break	45% XY / 28% Z
Thermal properties	
Melting temperature (20°C/min)	201°C
Heat deflection temperature (1.80 MPa)	46°C
Heat deflection temperature (0.45 MPa)	180°C
Physical properties	
Density	990 kg/m ³

Table 1.4 – Results for EOS Polyamide 11 (PA 1102 Black) [19]

1.4. Multi Jet Fusion – HP 3D printing technology

HP Multi Jet Fusion technology offers speed advantages and control over part and material properties beyond those found in other types of Powder Bed Fusion technologies [20].

The build begins by laying down a thin layer of powdered material across the working area. The material re-coater carriage scans from top-to-bottom [21]. Next, the printing and fusing carriage with an HP thermal inkjet (printhead) array and energy sources scans from right-to-left across the working area (see figure 1.11) [21]. The leading energy source preheats the working area immediately before printing to provide consistent and accurate temperature control of each layer as it is printed [21]. The printheads now print functional agents in precise locations onto the material to define the part's geometry and its properties. The printing and fusing carriage now returns left-to-right to fuse the areas that were just printed [21].

At the ends of the scans, supply bins refill the re-coater with fresh material (see figure 1.11), and service stations can test, clean, and service the printheads on the printing and fusing carriage as needed to ensure reliable operation [21].

After finishing each layer, the surface of the working area retracts about the thickness of a sheet of office paper, and the material re-coater carriage scans in the reverse direction for optimum productivity [21].

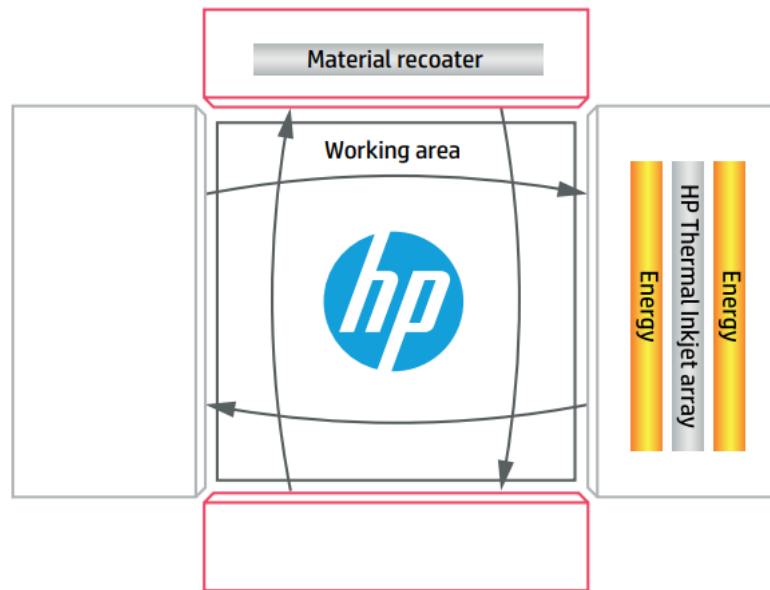


Figure 1.11 – Schematic of HP Multi Jet Fusion synchronous printing architecture [21]

The process continues layer-by-layer until a complete part, or set of parts is formed in the build unit (figure 1.12) [21].

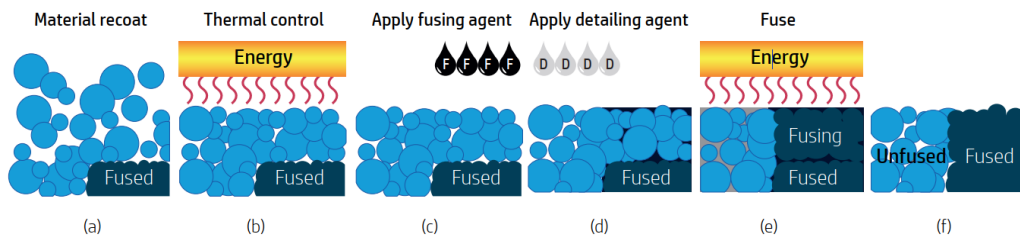


Figure 1.12 – Schematic of HP Multi Jet Fusion printing process, cross-sectional views (for each specific HP MJF machine model, some steps may differ in the process) [21]

The process begins by recoating the material in a thin layer across the work area, as shown schematically in figure 1.12 (a) [21].

figure 1.12 (b) represent what happens on the first scan of the printing and fusing carriage. The temperature at multiple points across the work area has been measured, and in figure 1.12 (b) energy is applied to the fresh layer to control the material temperature immediately before printing agents [21].

In figure 1.12 (c), the fusing agent (“F”) is selectively printed where particles should be fused [21].

In figure 1.12 (d), the detailing agent (“D”) is selectively printed where the fusing action will be either reduced or amplified. In this example, the detailing agent reduces fusing at the boundary to produce a part with sharp and smooth edges.

In figure 1.12 (e), the material is exposed to fusing energy, and selected areas now fuse. The fused material bonds to the layer below if that layer was fused on a previous cycle. Because HP Multi Jet Fusion technology can produce parts with Z-axis tensile strength comparable to the tensile strength in the X and Y planes, it overcomes the limitation of reduced Z-axis strength found in some other 3D printing technologies [21].

figure 1.12 (f) shows the fused and unfused areas at the edge of a part. The working area now retracts in preparation for the next recoating, printing, and fusing cycle [21].

figure 1.12 is a general overview of the process steps in HP Multi Jet Fusion technology. In specific HP Jet Fusion 3D printers, the order of steps may be rearranged and additional agents such as transforming agents may be applied during printing [21].

One of the big potentials foreseen for multi Jet fusion is the possibility of adding Voxels during the printing phase. The 3D analog of the pixel is the voxel, for “volume element.” In 2D printing, pixels are arranged on a surface in a regular grid. In 3D printing, voxels are also printed in a regular 2D grid, and a voxel has depth. The voxels form a thin layer that is the image of a part’s cross-section, and many such layers are stacked to form a 3D object. Specifying the properties of each voxel defines a 3D-printed part point-by-point over its surfaces and within its volume [21].

An analogy between printing pixels in a monochrome image and printing voxels by conventional 3D technologies highlights the advanced capabilities of HP Multi Jet Fusion technology. In 2D printing, multiple inks (cyan, magenta, yellow, and

black) can be combined in pixels to print an image with a wide range of colors. Using multiple agents, HP Multi Jet Fusion prints voxels with a range of physical and functional properties including color [21].

Figure 1.13 shows a 2D pixel and two (2) 3D voxels printed in layers 80 microns thick. HP Multi Jet Fusion technology can print up to 1200 voxels per linear inch in each layer [21]. Figure 1.13 illustrates the analogy between monochrome 2D pixel printing and conventional 3D binary voxel printing [21]. HP Multi Jet Fusion voxels are shown in color to signify the potential of HP Multi Jet Fusion technology to take 3D printing to new levels [21]. The breakthrough of printing voxels whose properties can be individually controlled is made possible using HP’s transforming agents in the HP Multi Jet Fusion process [21].

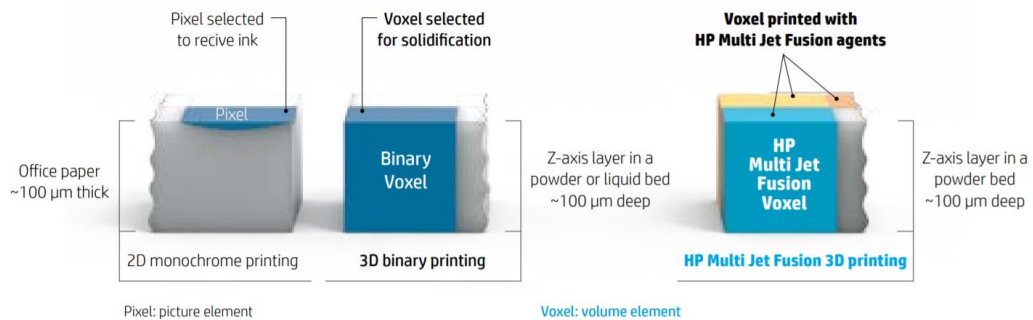


Figure 1.13 – Pixel, binary voxel, and HP Multi Jet Fusion voxels [21]

HP’s vision for HP Multi Jet Fusion technology is to create parts with controllably variable (even quite different) mechanical and physical properties within and across a single part or among separate parts printed simultaneously in the build unit [21]. This is accomplished using additional agents, which are called transforming agents, to control the interaction of the fusing and detailing agents with each other and with the material to be fused [21]. Depositing transforming agents voxel-by-voxel across each layer allows HP Jet Fusion 3D printers to produce parts that cannot be made by other methods [21].

In HP Jet Fusion 3D printers, properties that HP transforming agents could control within and across a part include (these properties may exist or not for each model of the HP jet fusion printer models) [21]:

- Dimensional accuracy and detail

- Surface roughness, texture, and friction coefficient
- Tensile strength, flexibility, hardness, and other material properties
- Electrical and thermal conductivity
- Opacity or translucency in plastics
- Color: embedded and at the surface

Figure 1.14 shows parts made by an HP Jet Fusion 3D printer that can print with color. Transforming agents print combinations of CMYK primary colors in each voxel. Color can be 3-dimensional—within the part or on its surface—to produce visible indications when the material is removed by wear or damaged [21]. This allows visual inspection to determine if a part must be replaced, and an embedded color can provide anti-tampering features [21]. In addition to visible colors, materials that emit specific colors only when illuminated by ultraviolet light (e.g., quantum dots and fluorescent dyes) can provide unobtrusive or hidden text and codes for security, identification, and other purposes [21].



Figure 1.14 – Sample parts made by HP Multi Jet Fusion technology [21]

HP MJF Polymer Materials:

Today, the main 3D Printing materials used in the HP Jet Fusion printers are “HP 3D High Reusability PA 12”, “HP 3D High Reusability PA 12 Glass Beads”, “HP 3D High Reusability PA 11” and “HP 3D High Reusability PP enabled by BASF”. (the data about mechanical properties of the materials in this chapter are presented by the manufacturers and they are not necessarily the same values obtained from the experiments carried out in Politecnico di Torino laboratories; this thesis experimental results are available in the “Results” chapter).

1. HP 3D High Reusability PA 12 is ideal for producing strong, quality parts at a low cost per part [22]. It provides good chemical resistance to oils, greases, aliphatic hydrocarbons, and alkalies [22]. Its biocompatibility meets USP Class I-VI and US FDA guidance for Intact Skin Surface Devices, and it achieves watertight properties without any additional post-processing [22]. HP Jet Fusion 3D Printing Solutions using HP 3D High Reusability PA 12 provide up to 80% powder reusability ratio, producing functional parts batch after batch [23].

	Value	Method
Powder melting point (DSC)	187° C 369° F	ASTM D3418
Particle size	60 µm	ASTM D3451
Bulk density of powder	0.425 g/cm ³ 0.015 lb/in ³	ASTM D1895

Table 1.5 – HP 3D High Reusability PA 12 characteristics [22]

HP 3D HR PA 12 ^{i,iii}	Average (XY)	Average (Z)	Test Method
Tensile strength (MPa) ^v	50	50	ASTM D638
Tensile modulus (MPa) ^v	1700	1900	ASTM D638
Elongation at yield (%)	12	8	ASTM D638
Elongation at break (%)	17	9	ASTM D638
Impact strength (kJ/m ²) ^v	3.7	3.8	ASTM D256
Density (g/cm ³)	1.01		ASTM D792
<i>i. Based on internal testing and measured using the HP Half_Commercial_Datasheet_Job. Results may vary with other jobs and geometries.</i> <i>ii. Using HP 3D HR PA 12 material, 20% refresh ratio, Balanced print profile, natural cooling, and measured after bead-blasting with glass beads at 5-6 bars.</i> <i>iii. Following all HP-recommended printer setup and adjustment processes and printheads aligned using semi-automatic procedure.</i> <i>iv. Tensile strength typical variation (95% of parts) falls within the 45-55 MPa range, while tensile modulus values remain within the 1500 to 2100 MPa range.</i> <i>v. Using the Izod test method A with notched @ 3.2 mm specimen according to the ASTM D256 standard.</i>			

Table 1.6 – Results for HP 3D High Reusability PA 12 [23]

2. HP 3D High Reusability PA 11 provides up to 70% powder reusability ratio [23]. It provides excellent chemical resistance and enhanced elongation-at-break. With high impact resistance properties and ductility, it is good to use for prostheses, insoles, sports goods, snap fits, living hinges, and more [22]. Its biocompatibility meets USP Class I-VI and US FDA guidance for Intact Skin Surface Devices [22].

	Value	Method
Powder melting point (DSC)	202° C 396° F	ASTM D3418
Particle size	54 µm	ASTM D3451
Bulk density of powder	0.48 g/cm ³ 0.017 lb/in ³	ASTM D1895

Table 1.7 – HP 3D High Reusability PA 11 characteristics [22]

HP 3D HR PA 11 ^{i,ii,iii}	Average (XY)	Average (Z)	Test Method
Tensile strength (MPa) ^{iv}	52	54	ASTM D638
Tensile modulus (MPa) ^{iv}	1700	1900	ASTM D638
Elongation at yield (%)	25	19	ASTM D638
Elongation at break (%)	36	25	ASTM D638
Impact strength (kJ/m ²) ^v	6	5	ASTM D256
Density (g/cm ³)	1.05		ASTM D792

i. Based on internal testing and measured using the HP Half_Commercial_Datasheet_Job. Results may vary with other jobs and geometries.
ii. Using HP 3D HR PA 11 material, 30% refresh ratio, Balanced print profile, natural cooling, and measured after bead-blasting with glass beads at 5-6 bars.
iii. Following all HP-recommended printer setup and adjustment processes and printheads aligned using semi-automatic procedure.
iv. Tensile strength typical variation (95% of parts) falls within the 48-56 MPa range, while tensile modulus values remain within the 1500 to 2100 MPa range.
v. Using the Izod test method A with notched @ 3.2 mm specimen according to the ASTM D256 standard.

Table 1.8 – Results for HP 3D High Reusability PA 11 [23]

3. HP 3D High Reusability PA 12 Glass Beads provide up to 70% powder reusability ratio [23]. 40% glass bead-filled thermoplastic material with both optimal mechanical properties and high reusability [22]. It is ideal for applications requiring high stiffness like enclosures and housings, fixtures, and tooling [22].

	Value	Method
Powder melting point (DSC)	186° C 367° F	ASTM D3418
Particle size	58 µm	ASTM D3451
Bulk density of powder	0.48 g/cm ³ 0.017 lb/in ³	ASTM D1895

Table 1.9 – HP 3D High Reusability PA 12 Glass Beads characteristics [22]

HP 3D HR PA 12 GB ⁱⁱⁱ	Average (XY)	Average (Z)	Test Method
Tensile strength (MPa) ^v	29	30	ASTM D638
Tensile modulus (MPa) ^v	2600	3000	ASTM D638
Heat deflection temperature [@ 0.45 MPa, 66 psi] (°C) ^{vii}	170	172	ASTM D648
Heat deflection temperature [@ 1.82 MPa, 264 psi] (°C) ^{vii}	110	120	ASTM D648
Elongation at yield (%) ^v	9	4	ASTM D638
Elongation at break (%) ^v	10	5	ASTM D638
Impact strength (kJ/m ²) ^{vi}	3	3	ASTM D256
Density (g/cm ³)	1.3		ASTM D792

i. Based on internal testing and measured using the HP Half_Commercial_Datasheet_Job. Results may vary with other jobs and geometries.
ii. Using HP 3D HR PA 12 GB material, 30% refresh ratio, Balanced print profile, natural cooling, and measured after bead-blasting with glass beads at 5-6 bars.
iii. Following all HP-recommended printer setup and adjustment processes and printheads aligned using semi-automatic procedure.
iv. Tensile strength typical variation (95% of parts) falls within the 28-32 MPa range, while tensile modulus values remain within the 2600 to 3200 MPa range.
v. Tensile test type I specimens measured with a pulling speed of 5 mm/min to comply with ASTM D638 test standards.
vi. Using the Izod test method A with notched @ 3.2 mm specimen according to the ASTM D256 standard.
vii. Using a standard bar specimen measuring 5" x 1/2" x 1/4" in accordance with ASTM D648.

Table 1.10 – Results for HP 3D High Reusability PA 12 Glass Beads [23]

4. HP 3D High Reusability PP enabled by BASF (polypropylene material) provides up to 90% powder reusability ratio [24]. Versatile material ideal for a wide range of automotive, industrial, and consumer goods applications [22]. It has excellent chemical resistance and low moisture absorption ideal for piping or fluid systems and containers with outstanding welding capabilities with other PP parts produced with traditional methods like injection molding [22].

	Value	Method
Powder melting point (DSC)	138° C 280° F	ASTM D3418
Particle size	62 µm	ASTM D3451
Bulk density of powder	0.34 g/cm ³ 0.012 lb/in ³	ASTM D1895

Table 1.11 – HP 3D High Reusability PP characteristics [22]

	Average (XY)	Average Z	Test Method
Tensile strength (MPa) ^{iv,v}	30	30	ASTM D638
Tensile modulus (MPa) ^{iv,v}	1600	1600	ASTM D638
Heat deflection temperature [@ 0.45 MPa, 66 psi] (°C) ^{vii}	100	100	ASTM D648
Heat deflection temperature [@ 1.82 MPa, 264 psi] (°C) ^{vii}	60	60	ASTM D648
Elongation at yield (%) ^v	10	10	ASTM D638
Elongation at break (%) ^v	20	18	ASTM D638
Impact strength (kJ/m ²) ^{vi}	3.5	3.0	ASTM D256
Density (g/cm ³)	0.89		ASTM D792
<p><i>i. Based on internal testing and measured using the HP Half_Commercial_Datasheet_Job. Results may vary with other jobs and geometries.</i></p> <p><i>ii. Using HP 3D HR PP enabled by BASF material, 20% refresh ratio, Balanced print profile, natural cooling, and measured after bead-blasting with glass beads (70–110 μm) at 5–6 bars.</i></p> <p><i>iii. Following all HP-recommended printer setup and adjustment processes and printheads aligned using semi-automatic procedure.</i></p> <p><i>iv. Tensile strength typical variation (95% of parts) falls within the 28–32 MPa range, while tensile modulus values remain within the 1360 to 1840 MPa range.</i></p> <p><i>v. Tensile test type I specimens measured with a pulling speed of 5 mm/min to comply with ASTM D638 test standards.</i></p> <p><i>vi. Using the Izod test method A with notched @ 3.2 mm specimen according to the ASTM D256 standard.</i></p> <p><i>vii. Using a standard bar specimen measuring 5" x 1/2" x 1/4" in accordance with ASTM D648.</i></p>			

Table 1.12 – Results for HP 3D High Reusability PP [24]

The HP Multi Jet Fusion Open Platform enables materials partners including Arkema, BASF, Lehmann & Voss Co., Evonik, and others to participate in the development of new HP Multi Jet Fusion materials [25].

2. Experimental Analysis

2.1. The SLS Machine

EOS GmbH Electro Optical Systems has improved its productivity rate in its new SLS 3D printer FORMIGA P 110 Velocis (Figure 2.1) with a Production Volume of 16.5 Liter [26]. They have made some innovations in temperature management and software control accelerate the heating and recoating process significantly increasing productivity [26]. The running costs are only consumed material and power, and no agents are used during production [26].



Figure 2.1 – SLS 3D Printer FORMIGA P 110 Velocis [26]

The precise laser spot with a small focus diameter enables wall thicknesses of less than a half millimeter [26]. The system reliably produces small, delicate parts with the highest surface quality [26]. Parts are fully functional right after unpacking and depowering [26]. No further post-processing is needed. With 9 commercial polymer materials and 10 combinations of materials/layer thicknesses [26]. The EOS Parameter Editor allows customized exposure parameters to be defined based on a proven

baseline [26]. Some important technical data of the machine are introduced in table 2.1.

Technical Data FORMIGA P 110 Velocis	
Building volume	200 x 250 x 330 mm (7.9 x 9.8 x 13 in)
Laser type	CO ₂ ; 30 W
Building rate	up to 1.2 l/h
Layer thickness (depending on material)	0.06 – 0.10 – 0.12 mm (0.0024 – 0.0039 – 0.0047 in)
Precision optics	F-theta lens, high-speed scanner
Scan speed during build process	up to 5 m/s (16.4 ft/s)
Power supply	16 A
Power consumption	typical 3 kW, maximum 5 kW
Dimensions (W x D x H)	1,320 x 1,067 x 2,204 mm (51.97 x 42.01 x 86.77 in)
Recommended installation space	min. 3.2 x 3.5 x 3.0 m (126 x 138 x 118 in)
Weight	approx. 600 kg (1.323 lb)

Table 2.1 – Technical Data for FORMIGA P 110 Velocis AM machine [26]

In Table 2.2, the EOS Portfolio of the most common EOS SLS Polymer Materials is available. Depending on the desired part properties and considering the production cost with each of these materials, one of them can be chosen.

Product class	Product name	Colour of lasersintered parts	Main properties	Typical applications
Polyamide 12	PA 2200	white	→ Multipurpose material → Balanced property profile	Functional parts
	PA 2202 black	anthracite black	→ Balanced property profile → Pigmented throughout	Functional parts
Polyamide 12, glass bead filled	PA 3200 GF	whitish	→ High stiffness → Wear resistance → Improved temperature performance	Stiff housings Parts with requirements on wear and abrasion Parts used under elevated thermal conditions
Polyamide 12, aluminium filled	Alumide®	metallic grey	→ Easy post-processing, good machinability → High temperature performance → Thermal conductivity (limited) → High stiffness	Applications with metallic finish Parts requiring machining Parts with thermal loads
Polyamide 11	PA 1101	natural	→ High ductility and impact resistance → Otherwise balanced property profile (similar to PA 2200) → From renewable sources	Functional parts requiring impact resistance Parts with functional elements like film hinges
	PA 1102 black	black	→ Similar properties as PA 1101 → Mass-coloured, parts remain black even under abrasive wear	Similar to typical applications for PA 1101

Table 2.2 – EOS SLS Polymer Materials portfolio selection guide [27]

In Figure 2.2, the materials which are compatible with the SLS 3d printer FORMIGA P 110 Velocis are visible.

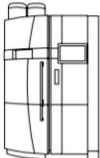
		Product name
		Layer thickness
	Polyamide 12 PA 2200® 60 100 120 μm	Polyamide 11 PA 1101 100 μm
	PA 2201 100 μm	PA 1102 black 100 μm
	PA 3200 GF 100 μm	Polypropylene PP 1101 100 μm
	Alumide® 100 μm	Polystyrene PrimeCast®101 100 μm
	FORMIGA P 110 Velocis	

Figure 2.2 – Compatible materials with the SLS 3d printer FORMIGA P 110 Velocis [27]

2.2. The MJF Machine

“HP Jet Fusion 4200 3D Printing Solution” (figure 2.3) which is only one of the available AM machines in the FCA EMEA PD Additive Manufacturing Centre, is the other AM technology used for producing the specimens necessary to carry out the comparison about the mechanical properties in this thesis.



Figure 2.3 – HP Jet Fusion 4200 3D Printing Solution [28]

The general printing procedure of a Multi Jet Fusion was described in the last chapter; however, those steps can vary between different HP 3D printer models available in the market. The Printing procedure until completion of the job in the specific choice of “HP Jet Fusion 4200” is as follows [20]:

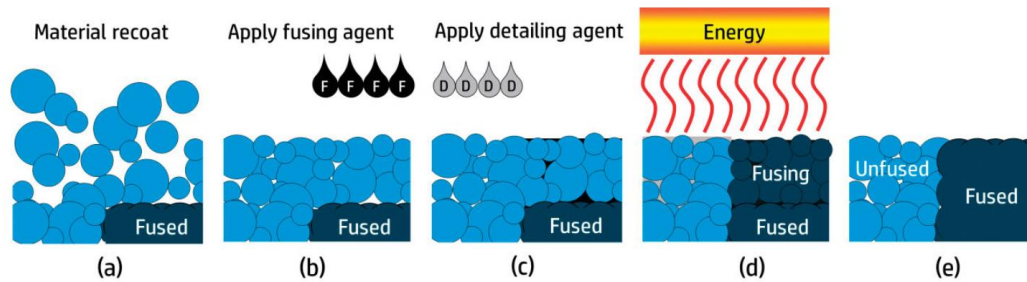


Figure 2.4 – Schematics of HP Jet Fusion 4200 printing procedure [20]

- The material is recoated across the work area.
 - A fusing agent (F) is selectively applied where the particles are to fuse.
 - A detailing agent (D) is selectively applied where the fusing action needs to be reduced or amplified. In this example, the detailing agent reduces fusing at the boundary to produce a part with sharp and smooth edges.
 - The work area is exposed to fusing energy.
 - The part now consists of fused and unfused areas.
- The process is repeated until the complete part has been formed.

Printing and cooling times must be considered when scheduling the final job for printing [20]. Printing and cooling times vary depending on the part size and number of parts in each printing session [20]. As a general guide for a full build chamber, expect around 16 hours of printing and 46 hours of cooling. [20] Cooling times are approximate and may vary a lot depending on the complexity of the build and if the fast cooling is integrated into the system or not [20]. For having more details, some more information is available on the printing and cooling time table (see table 2.3) [20]. with the minimum Natural cooling time listed on the table, there is a need to use heat-resistant gloves and goggles for unpacking the build unit [20].

Build chamber	Printing time		Safety cooling time	Natural cooling time		Fast cooling time *
	Fast print mode	Default/Strength print mode		Normal	Minimum *	(in systems with fast cooling integrated)
100% full	10 h	16 h 20 min	20–30 min	46 h	31 h	10 h
75% full	7 h 30 min	12 h 15 min	20–30 min	35 h	23 h	8 h
50% full	5 h	8 h 10 min	20–30 min	23 h	16 h	6.5 h
25% full	2 h 30 min	4 h	20–30 min	12 h	8 h	5 h

Table 2.3 – HP Jet Fusion 4200 3D printing and cooling time [20]

For preparing the job and sending it to be printed, the powerful 3D print-preparation capabilities of HP SmartStream 3D Build Manager is used [20]. The software creates slices that the printer can convert to layers to prepare the job [20]. This preparation process may take from 15 minutes to 2 hours depending on the complexity of the job [20]. It can be done while printing other jobs. Once ready, you can select the job to be printed from the job queue on the printer’s front panel [20]. The steps are as follows [20]:

1. Add parts to begin preparing the print job.
2. Rotate, size, and position the part on the bed.
3. Automatically locate and fix 3D geometry errors.
4. Send a printer-ready file to a connected 3D printer or save the printable file.

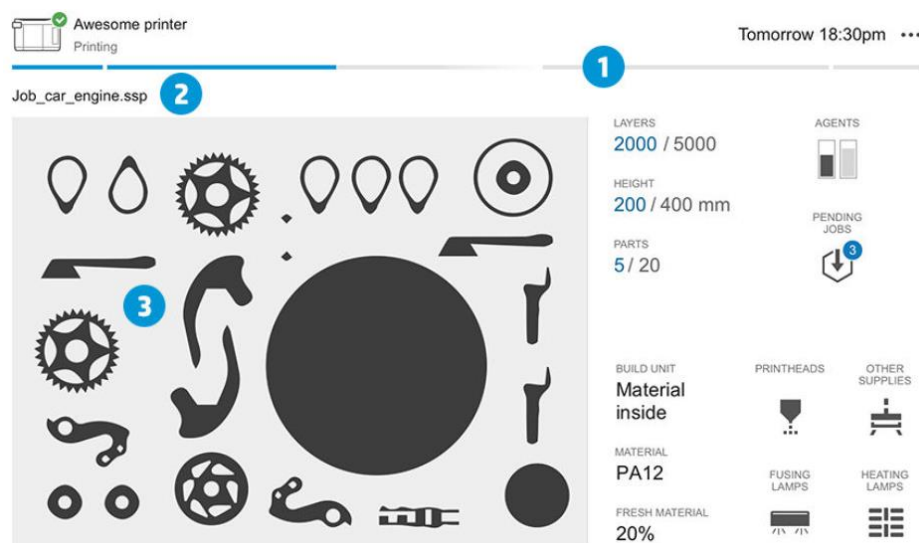
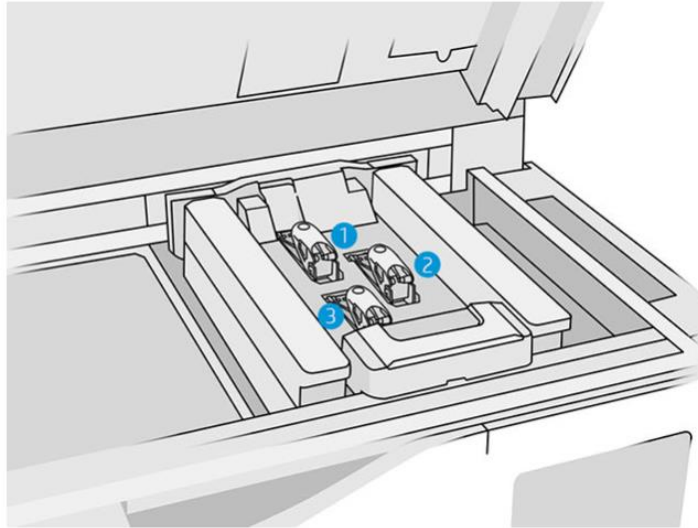


Figure 2.5 – HP SmartStream 3D Build Manager user interface
1- Progress bar showing the progress of the build, 2- Job name,
3- Job cross-section image showing the slice currently printing [20]

There are two kinds of agents: fusing and detailing agents [20]. The printheads take agents and deposit them on the build [20]. The printer's writing system uses three dual-agent printheads with 31,680 nozzles each; consequently, each agent has 15,840 nozzles. The printheads are numbered as shown in figure 2.6 [20].



*Figure 2.6 – HP Jet Fusion 4200 printheads
1- Rear printhead, 2- Middle printhead, 3- Front printhead [20]*

The HP Jet Fusion 4200 and 4210 accept cartridges with a capacity of 30 or 300 liters [20].

Material states in the processing station are as follows [20]:

- Reusable: Material that can be reused
- Waste material: Used material that should not be reused
- Mixed: A mixture of new and used material, by default 20% new and 80% used
- Fresh: New material

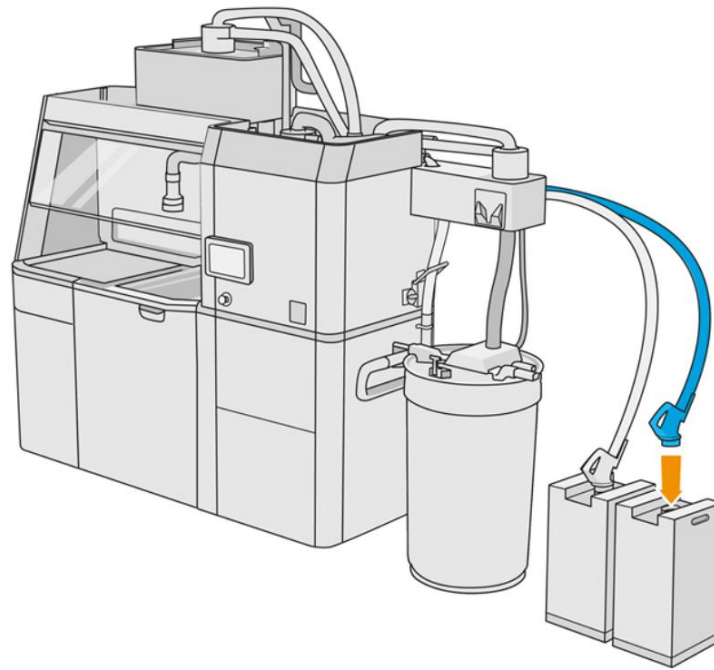


Figure 2.7 – HP Jet Fusion 4200 cartridges [20]

There are some specifications (the minimum specification for parts) to bear in mind to avoid issues in parts and to achieve the best quality (figure 2.8) [20].

The minimum printable features in planes X, Y, and Z are as follows [20]:

Minimum hole diameter at 1 mm thickness	0.5 mm
Minimum shaft diameter at 10 mm height	0.5 mm
Minimum printable font size for embossed or debossed letters or numbers:	6 pt
Minimum clearance at 1 mm thickness	0.5 mm
The minimum slit between walls	0.5 mm

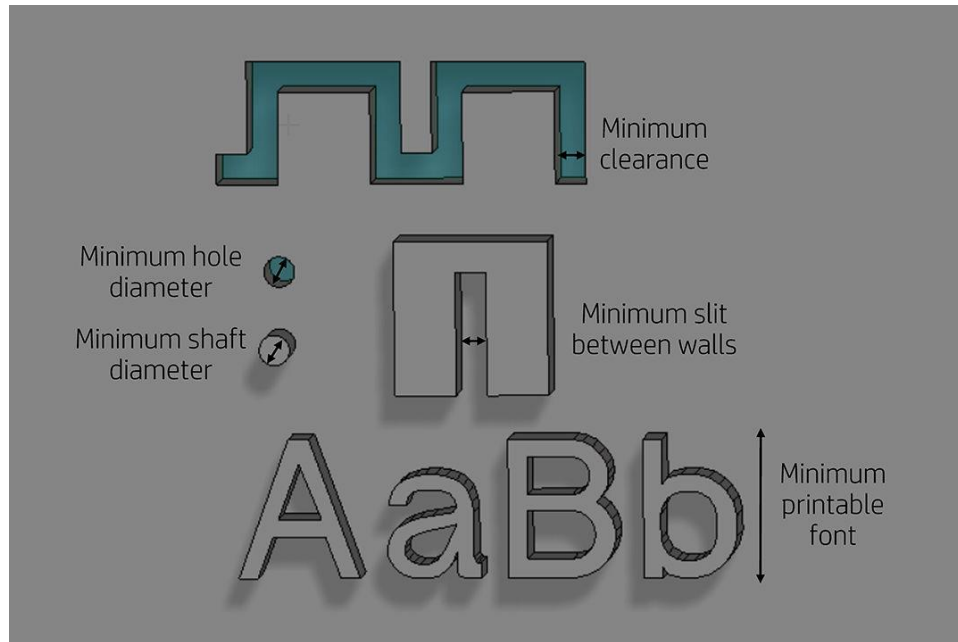


Figure 2.8 – HP Jet Fusion 4200 minimum printable features in planes X, Y, and Z [20]

In the HP SmartStream 3D Build Manager, you can choose one of the following print modes from the print profile drop-down menu, depending on your needs [20]:

- The balanced mode delivers balanced properties.
- Fast mode maximizes speed for any job, available for certain materials.
- Mechanical mode delivers superior stain-resistant properties, available for certain materials.
- Cosmetic mode delivers higher accuracy, a smoother surface, and better color uniformity, available for certain materials.

	Balanced PM	Mechanical PM	Fast PM	Cosmetic PM
PA12	X	X	X	X
PA11	X	X	X	
PA12GB	X			

Table 2.4 – HP Jet Fusion 4200 3D printing speed options considering the powder type [20]

In the case of Natural cooling, move the build unit aside to cool down further, and wait [20]. The cooling time depends on the size of the build [20]. After, the build unit has to be inserted into the processing station [20].

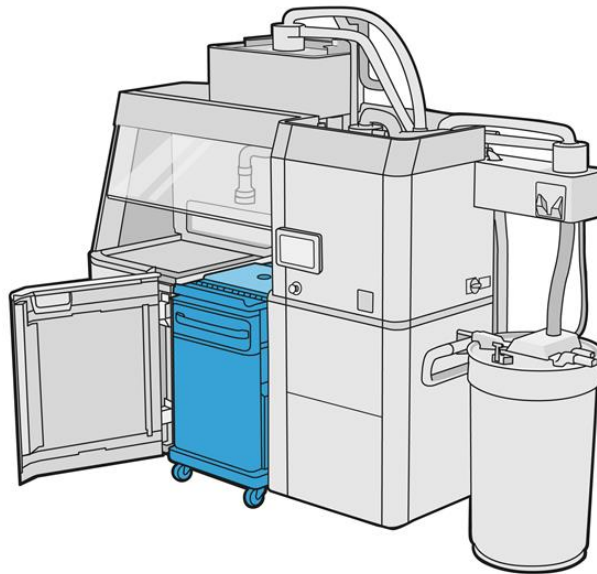


Figure 2.9 – HP Jet Fusion 4200 processing station [20]

In the case of Fast cooling, the procedure described below must be followed [20]:

- a. The build unit must be left to cool naturally for 3 or 4 hours before fast cooling can start. It does not need to be inside the processing station during this time.
- b. When the build unit has been inserted into the processing station (figure 2.9), go to the processing station’s front panel, and tap Build unit > Fast cooling.
- c. Fast cooling starts. By tapping at X at any time, fast cooling is canceled. To resume the process, ensure that the build unit is inserted, and tap Fast cooling. Before starting the fast cooling process, you can modify the timing by tapping Modify, however, modifying this value may compromise part quality.

Default cooling times for PA12 material

	Fast cooling	Natural cooling (to reach 80°C)
Half-full build chamber (190 mm)	6.9 h	18.4 h
Full build chamber (380 mm)	9.4 h	33.4 h

Table 2.5 – HP Jet Fusion 4200 3D natural and fast cooling processes time [20]

- d. Connect the reusable material collector to the safety lid (see figure 2.10), and tap Start on the front panel, which will tell you the remaining time.

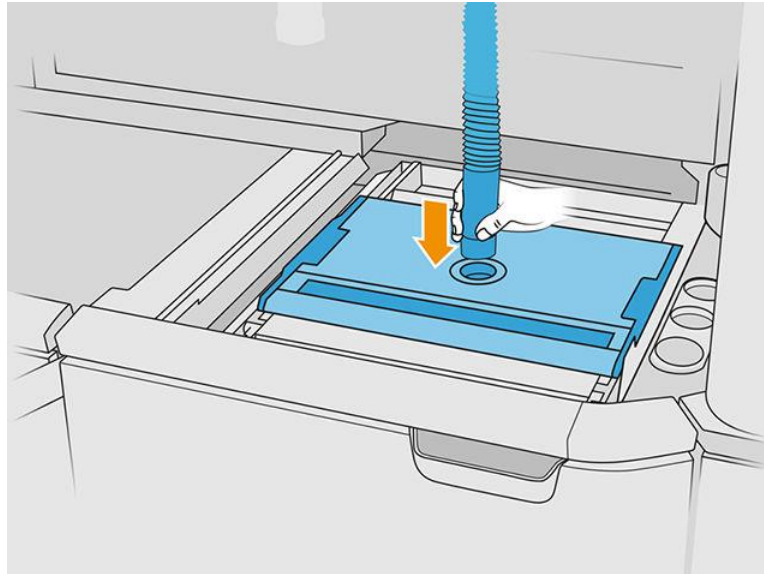


Figure 2.10 – HP Jet Fusion 4200 processing station reusable material collector [20]

Part cleaning and postprocessing [20]:

Once parts have been unpacked from the build in the processing station, they should be cleaned [20]. Different processes can be followed, depending on the needs. In general, equipment not provided by HP are needed [20]. The main process recommended by HP is a combination of bead blasting (first) and air blasting (second) [20].

- **Bead blasting:** It consists of applying compressed air mixed with an abrasive to the part to remove the attached material. This is a generally appropriate solution; however, different abrasives or pressures for specific purposes should be selected [20].
- **Air blasting:** This process consists of applying compressed air to the part to remove any material remaining after bead blasting [20].

The following options are available to improve surface finishing [20]:

- **Tumbling:** The part is immersed in a Vibro-tumbler full of abrasives, to smooth any surface roughness [20].
- **Hand sanding:** The surfaces of the part are smoothed by abrasion with sandpaper [20].

In Table 2.6, the HP 3D Printing materials portfolio selection guide is available. Depending on the desired part properties and considering the production cost with each of these materials, one of them can be chosen.

Usage and properties	HP 3D HR PA 11	HP 3D HR PA 12	HP 3D HR PA 12 GB	VESTOSINT® 3D Z2773 PA 12 ¹³	ESTANE® 3D TPU M95A
Visual aids & presentation models	●	●	●	●	●
Functional prototyping	●	●	●	●	●
End-use parts	●	●	●	●	●
Dimensional stability	●	●	●	●	●
Functional rigid part (higher stiffness)	●	●	●	●	●
Ductile part (higher elongation at break)	●	●	●	●	●
Impact	●	●	●	●	●
HDT (heat deflection temperature)	●	●	●	●	●
Medical biocompatibility ⁹ (USP Class I-VI and US FDA guidance for Intact Skin Surface Devices)	●	●	●	●	●
Look and feel	●	●	●	●	●

● Excellent ● Good ● Fair ● Not recommended ● In testing

Table 2.6 – HP 3D Printing materials portfolio selection guide [29]

2.3. The AM Material PA 12

In this section, the detailed information regarding the PA12 used for producing the specimens by the HP Jet Fusion 4200 3D Printer and SLS 3D Printer FORMIGA P 110 Velocis is presented.

The PA 12 material used by Multi Jet Fusion technology has a very fine grain, resulting in parts with higher density and lower porosity than parts produced with Laser Sintering [30]. That feature also makes PA 12 for MJF the ideal choice when you need more detailed surface resolution or thinner walls than are possible with Laser Sintering [30]. Unfinished parts typically have a smooth surface, without visible layers, and a stone-grey color [30].

The material datasheet is available in Table 2.7.

MEASUREMENT	VALUE	STANDARD
Density of parts	1.01 g/cm ³	ASTM D792
Tensile Strength, Max Load - XY	48 MPa/6960 psi	ASTM D638
Tensile Strength, Max Load - Z	48 MPa/6960 psi	ASTM D638
Tensile Modulus - XY	1700 MPa/245 ksi	ASTM D638
Tensile Modulus - Z	1800 MPa/260 ksi	ASTM D638
Elongation at Break - XY	20%	ASTM D638
Elongation at Break - Z	15%	ASTM D638
Heat Deflection Temperature - Z	175 °C 95 °C	ASTM D648 @ 0.45 MPa @ 1.82 MPa

Table 2.7 – HP MJF PA 12 material datasheet [30]

Among several types of EOS Polyamide 12, PA 2200 is one of the most common choices. The property profile of durable white parts made from PA 2200 is very balanced; such parts are characterized by strength, rigidity, and good chemical resistance [18]. They are also biocompatible and certified for contact with foodstuffs [18].

The Technical data reported by the producer is available in table 2.8. It should be reminded that the mechanical properties in additive manufacturing depend on several parameters, such as the printing material used, the x-, y-, z-position during the production (and also the combination of the other orientations), and the exposure parameters used. The influence of the orientation and the positioning of the parts during the printing phase in the build volume (on mechanical properties) is reported in this thesis for the technologies of the debate.

Material data sheet (PA 2200)

Average grain size	ISO 13320-11	56	µm
	Laser diffraction	2.20	mil
Bulk density	EN ISO 60	0.45	g/cm ³
Density of laser-sintered part	EOS method	0.93	g/cm ³
		58	lb/ft ³
Tensile modulus	EN ISO 527	1700	MPa
	ASTM D638	247	ksi
Tensile strength	EN ISO 527	48	MPa
	ASTM D638	6962	psi
Elongation at break	EN ISO 527	24	%
Elongation at break	ASTM D638	24	%
Flexural modulus	EN ISO 178	1500	MPa
	ASTM D790	217	ksi
Melting point	EN ISO 11357-1	172 - 180	°C

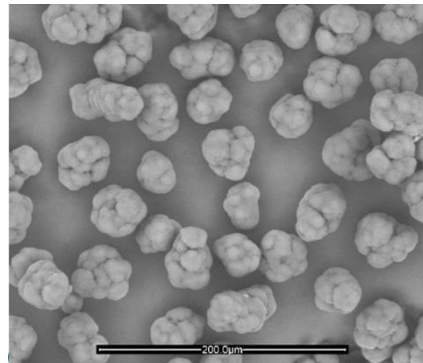
Table 2.8 – EOS PA 12 (PA 2200) material datasheet [31]

The following powders were observed under the scanning electron microscope (see Figure 2.11), SEM (ESEM, Quanta FEI, Eindhoven, The Netherlands, operated in high vacuum mode), and chemically analyzed using X-ray Energy Dispersion Spectroscopy, X-EDS (Oxford INCA-350, GB):

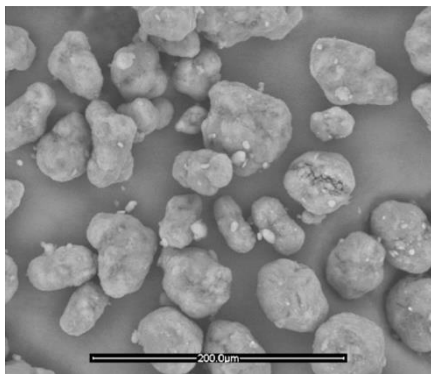
- PA12, reference (“PA12_ref”)
- PA12 from EOS for selective laser sintering, SLS (“PA12_EOS”)
- HP MJF PA12 powder (“PA12_MJF”)

The particles of the reference powder, PA12_ref (Figure 2.11_a), are globular and uniform in size, with a peculiar cauliflower-like morphology, Whereas the particles of PA12_EOS powder (Figure 2.11_b) and the PA12_MJF powder (Figure 2.11_c), are both less roundish and less even in size compared to the PA12_ref, and their surface is scaly. However, the PA12_EOS particles are slightly more regular than the PA12_MJF ones.

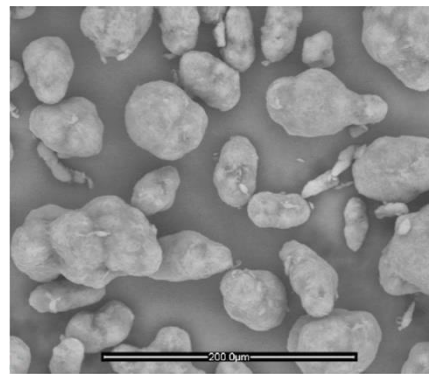
Under higher magnification, some broken particles of PA12_EOS clearly show they are the result of the aggregation of very small (micron-sized) particles.



(a) PA12, reference (“PA12_ref”)



(b) EOS PA12 (“PA12_EOS”)



(c) HP MJF PA12 (“PA12_MJF”)

Figure 2.11 – Morphology of PA powders: (a) PA12_ref, (b) PA12_EOS, and (c) PA12_MJF (scale bar: 200 μm)

3. Testing Information and Standards

3.1. The Tensile Test

One of the fundamental tests for determining the mechanical properties of a material is the tensile testing, also known as tension testing. In this test, a load is applied along the longitudinal axis of a test specimen (as shown in figure 3.1). The applied load and the resulting elongation of the member are measured and usually stored as a file for further analyzing and obtaining the so-called Stress-Strain diagram.

Load-deformation data obtained from tensile and/or compressive tests do not give a direct indication of the material behavior, because they depend on the specimen geometry [32]. The geometry of the Specimen used for each tensile test depends on the Standard we are following for the tensile test, which mainly depends on the type of material that we are investigating the properties. The cross-section of the Specimen can be rectangular or circular.

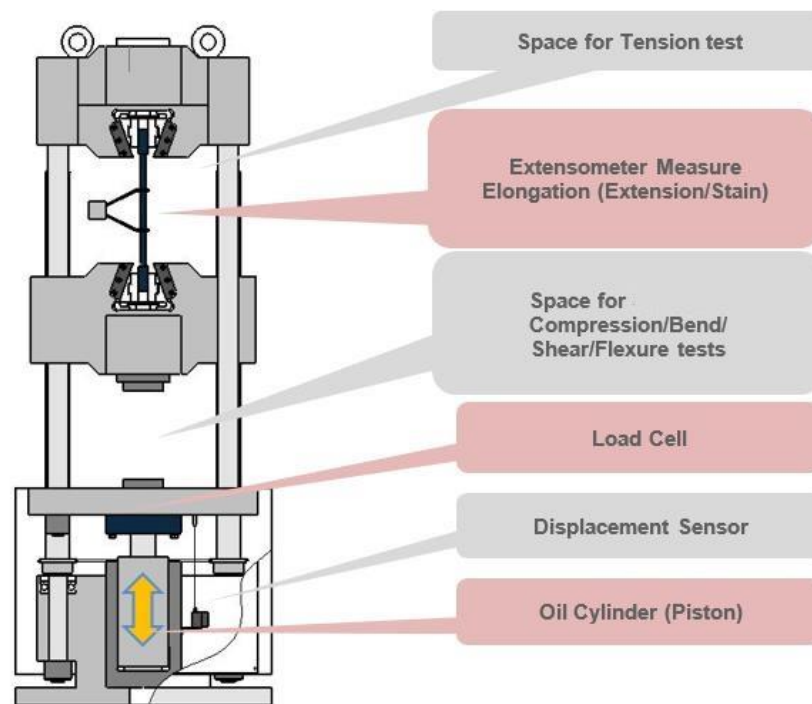


Figure 3.1 – Schematic diagram of Tensile Testing Machine [33]

After using the relationships below, loads and deformations may be converted to stresses and strains [32]:

$$\sigma = P/A$$

$$\epsilon = \delta/L$$

σ = normal stress on a plane perpendicular to the longitudinal axis of the specimen

P = applied load

A = original cross-sectional area

ϵ = normal strain in the longitudinal direction

δ = change in the specimen's gage length

L = original gage length

The resulting stress-strain curve or diagram gives a direct indication of the material properties [32]. Stress-strain diagrams are typically based upon the original cross-sectional area and the initial gage length, even though these quantities change continuously during the test [32]. These changes have a negligible effect except during the final stages of the test [32].

In Figure 3.2, the Load-deformation and the obtained Stress-strain diagram for 3 different Aluminum alloy specimens (2017-T451 Aluminum Alloy) [32]:

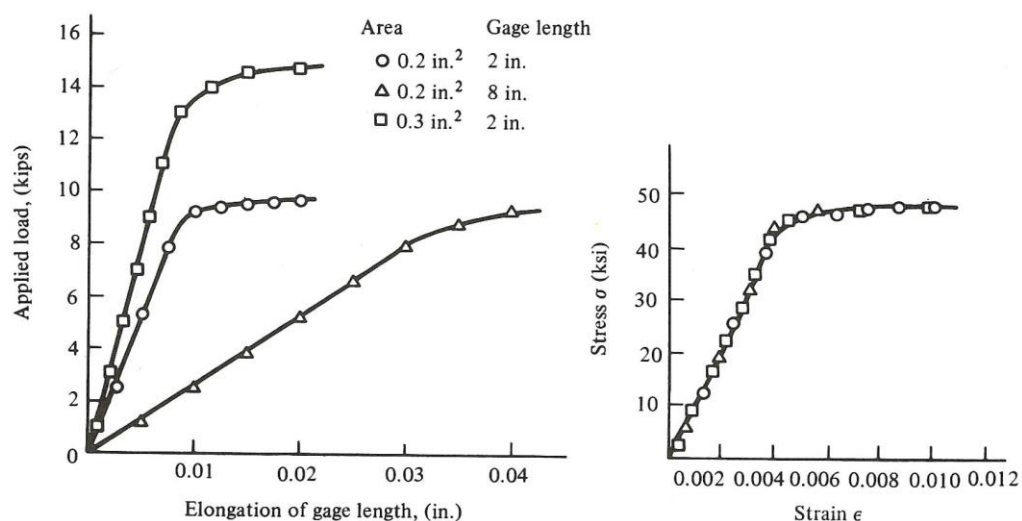


Figure 3.2 – Load-deformation and the obtained Stress-strain diagram for 3 Aluminum alloy specimens with different geometry (2017-T451 Aluminum Alloy) [32]

The first diagram from the left side shows the Load-deformation curve for three different specimens' types with different cross-section areas and different gage lengths [32]. However, as you can see in the other diagram, even with different specimens in the case of geometry, we will almost get the same stress-strain curve [32].

Engineering stress and engineering strain are computed using the original specimen dimensions, while True stress and true strain are based upon instantaneous values of cross-sectional area and gage length [32].

As shown in the previous diagram, the initial portion of the stress-strain diagram for most materials used in engineering structures is a straight line [32]. For the initial portion of the diagram, the stress σ is directly proportional to the strain ϵ [32]. Therefore, for a specimen subjected to a uniaxial load, we can write [32]:

$$\sigma = E\epsilon$$

This relationship above is known as Hooke's Law and was first recorded by Robert Hooke, an English mathematician, in 1678 [32].

It must be mentioned that Hooke's Law describes only the initial linear portion of the stress-strain curve for a specimen subjected to a uniaxial extension [32]. This section of the curve is under the elastic elongation only, and we do not have a plastic deformation [32].

The slope of the straight-line portion of the stress-strain diagram is called the Modulus of Elasticity or Young's Modulus [32].

$$E = \sigma/\epsilon \text{ (normal stress-strain)}$$

$$G = \tau/\gamma \text{ (shear stress-strain)}$$

E = Elastic Modulus or Modulus of Elasticity

G = Shear Modulus or Modulus of Rigidity

Some important material properties visible on the stress-strain curve are as follows (figure 3.3) [32]:

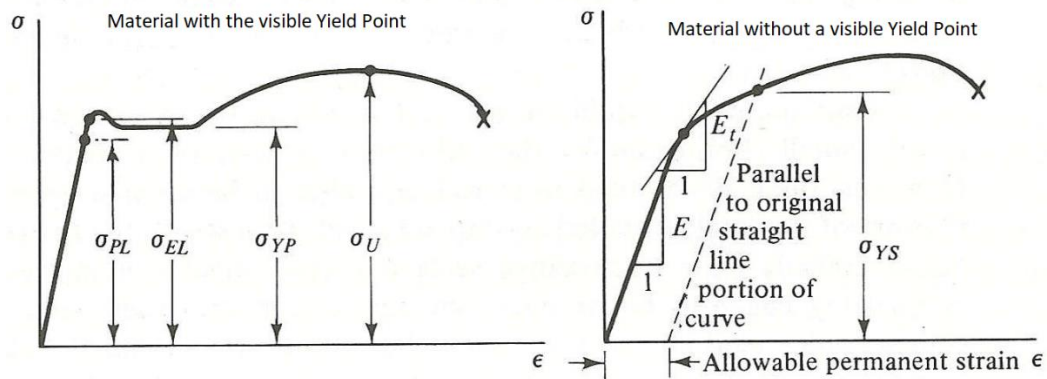


Figure 3.3 – The stress-strain curve of a material with the visible Yield Point (left), and without a visible Yield Point (right) [32]

$\sigma_{PL} \Rightarrow$ Proportional Limit - Stress above which stress is no longer proportional to the strain [32].

$\sigma_{EL} \Rightarrow$ Elastic Limit - The maximum stress that can be applied without resulting in permanent deformation when unloaded [32].

$\sigma_{YP} \Rightarrow$ Yield Point - Stress at which there are large increases in strain with little or no increase in stress. Among common structural materials, only steel exhibits this type of response [32].

$\sigma_{YS} \Rightarrow$ Yield Strength - The maximum stress that can be applied without exceeding a specified value of permanent strain [32].

Regarding the Offset Yield Point for the non-metallic and polymer materials, the offset allowable strain value can change. Regarding the yield point determination for the non-metallic and polymer materials, if the temperature of the testing environment is in the range of "the Glass Transition Temperature" (T_g), a 1% offset value is mostly used to find the approximate yield strength (see figure 3.4) [34].

The range the Glass Transition Temperature" (T_g) for the PA12 is from 297 to 314 Kelvin. Consequently, if we consider the IAM center environment temperature about 20 Celsius degrees, the assumption of using the 1% offset for the yield stress point is true.

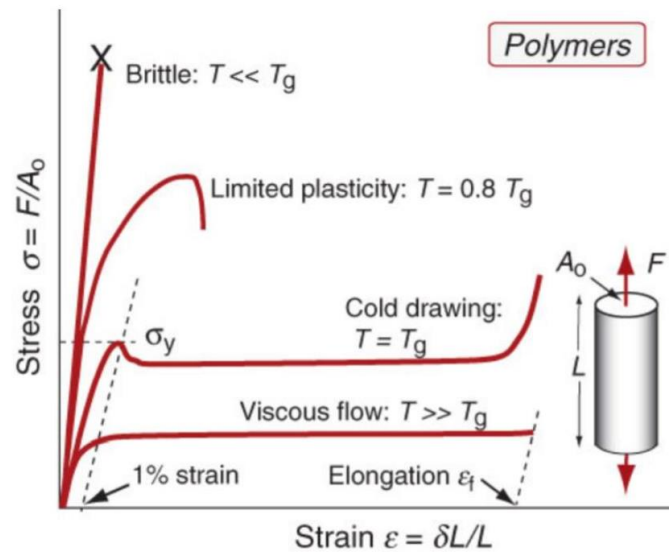


Figure 3.4 – Stress-strain curves for a polymer at T below and above the glass temperature [34]

$\sigma_U \Rightarrow$ Ultimate Strength - The maximum stress the material can withstand (based on the original cross-sectional area) [32].

$E \Rightarrow$ Modulus of Elasticity - Slope of the initial linear portion of the stress-strain diagram [32]. The modulus of elasticity may also be characterized as the “stiffness” or ability of a material to resist under elastic deformation within the linear range [32].

Percent Elongation - The strain at fracture in tension, expressed as a percentage = $((\text{final gage length} - \text{initial gage length}) / \text{initial gage length}) \times 100$. Percent elongation is a measure of ductility [32].

Materials can be divided into two broad categories (ductile materials and brittle materials) [32]:

Ductile Material: materials that can undergo large strain rates (at normal testing temperature) before failure [32].

Brittle Material: materials that fail in tension at relatively low values of strain [32].

Brittle materials fail due to normal tensile stresses and rupture occurs along a surface perpendicular to the load [32]. However, ductile materials usually fail on planes that correspond to the maximum shear stresses (45°) [32].

3.2. The Standards

The Standard considered for the tensile tests carried out in this thesis is: ISO 527-1; The International Standard on Plastics — Determination of tensile properties. There are various specimen types to use compatible with this standard, and each of them is adequate for a specific material or production type.

The chosen Standard for designing the specimens used for the tensile tests is: ISO 3167 type 1A; The International Standard on Plastic-multipurpose specimens.

The dimension of the test specimens:

Below, you can see a table available in the standard ISO 3167 type 1A in which you can find the details of the geometry for designing the specimen. All the dimensions are in millimeters (see figure 3.5 & table 3.1).

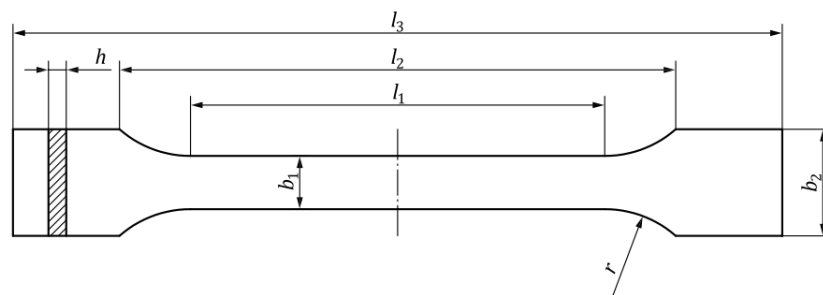


Figure 3.5 – The drawing of the specimen according to the ISO 3167 type 1A standard [35]

	Specimen type	A	B
l_3	Overall length ^a	≥ 150 Recommended value ^b 170	≥ 150
l_1	Length of narrow parallel-sided portion	80 ± 2	$60,0 \pm 0,5$
r	Radius	20 to 25 Recommended value ^b 24 ± 1	$\geq 60^c$ Recommended value ^b $60,0 \pm 0,5$
l_2	Distance between broad parallel-sided portions ^d	104 to 113	106 to 120 Recommended range ^b 106 to 110
b_2	Width at ends	$20,0 \pm 0,2$	
b_1	Width of narrow portion	$10 \pm 0,2$	
h	Thickness	$4,0 \pm 0,2$	

Table 3.1 – The details of the geometry of the specimen (ISO 3167 type 1A standard) [35]

The recommended overall length of 170 mm for type A is consistent with ISO 294-1 and ISO 10724-1 [35]. For some materials, the length of the tabs may need to be extended (e.g. to give an overall length of 200 mm) to prevent breakage or slippage in the jaws of the test machine [35].

The lower tolerances on the radius reduce the ranges of the stress concentrations that are found at the transitions between the narrow parallel-sided and the rounded portions [35]. Together with the smaller tolerance on the distance between the broad parallel-sided portions for type B, a common value of the initial distance between jaws can be used for tensile testing (see ISO 527-2).

The radius r can be obtained from the relation below [35]:

$$r = \frac{(l_2 - l_1)^2 + (b_2 - b_1)^2}{4(b_2 - b_1)}$$

l_2 , the distance between broad parallel-sided portions, is resulting from l_1 , r , b_1 , and b_2 , but within the indicated tolerance [35].

The drawing of the specimen by CATIA V5 and the final details of the geometry is available in figure 3.6.

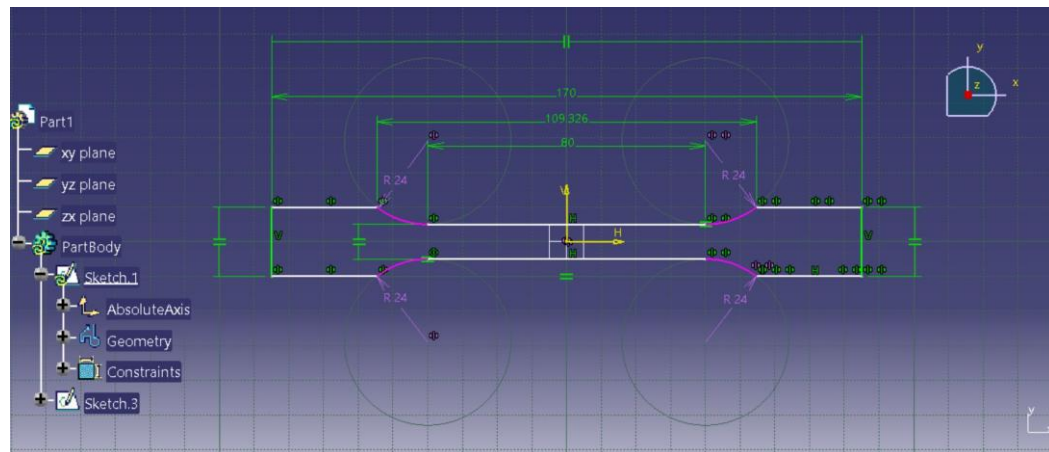


Figure 3.6 – The drawing of the used specimen in the thesis (ISO 3167 type 1A) in CATIA V5

It should be mentioned that the maximum 3d quality for CATIA V5 is used to get the smoothest curves and edges possible in the 3d design file. This can make a little improvement in the “.stl” format file used for the production phase with the AM machine. For a better understanding, in figure 3.7 the improvement of the curves and edges of the specimens after increasing the quality of the design in the

settings section of the designing program (CATIA V5) is visible in the “.stl” format files.

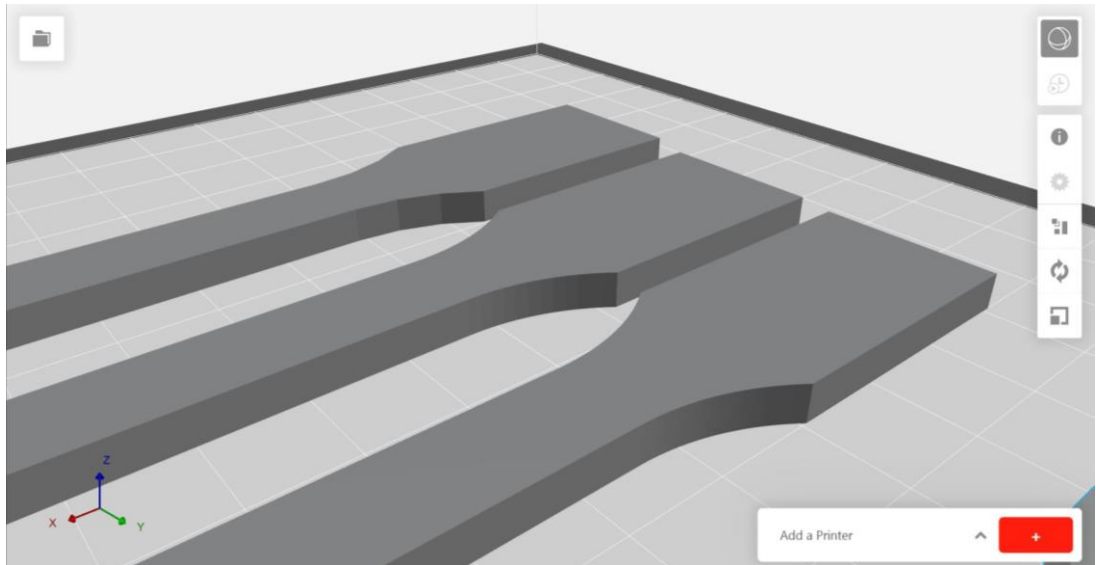


Figure 3.7 – The improvement of the “.stl” format files after increasing the edge quality of the design in CATIA V5, the surface design is smoother from theft to right

4. Results

4.1. Output data of the tensile test machine

For each technology of the debate, there are 45 specimens produced in 9 different orientations.

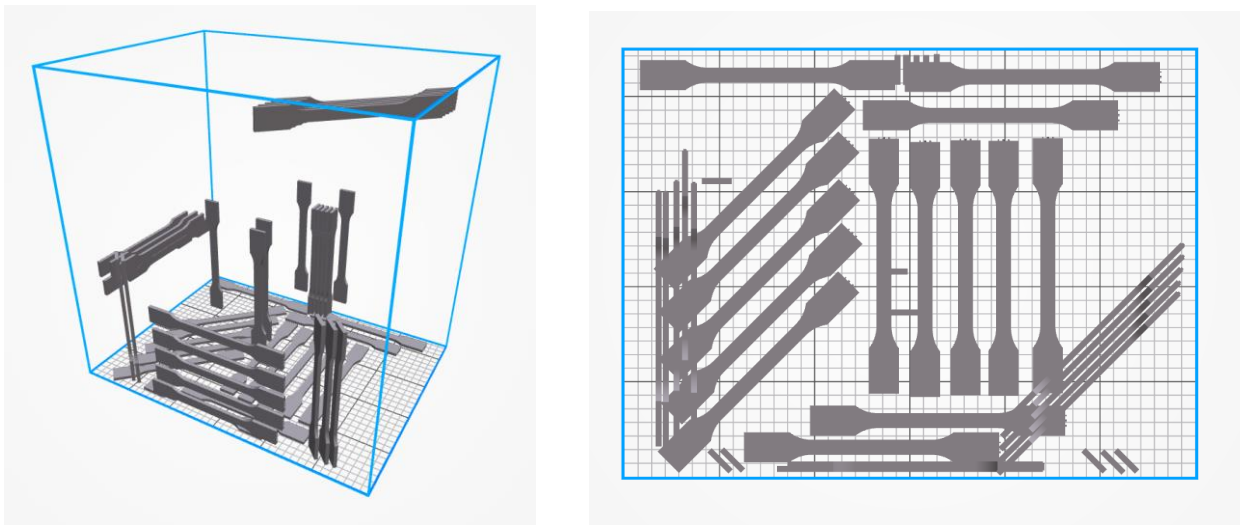


Figure 4.1 – The arrangement of the 45 specimens in the build volume of the HP Jet Fusion 4200 (380 x 284 x 380 mm), according to the designed orientations. Isometric-view (left) and bottom view (right)

For each technology of the debate, there are 45 specimens produced in 9 different orientations. Having 5 specimens tested for each specific printing orientation helps to get a trustable mean value for each of the mechanical properties through the tensile test.

Figure 4.2 shows the nine different positionings chosen for producing the specimens. This figure is only to specify the orientation and the given name to it, and it is not the build volume of the two machines. Each specimen has its name printed at one of the end-surfaces along its axis. Having the name of the specimen printed on it makes it easier to recognize it after the cleaning process, and

throughout the experimental phase when there are 45 specimens to undergo the tensile test for each technology.

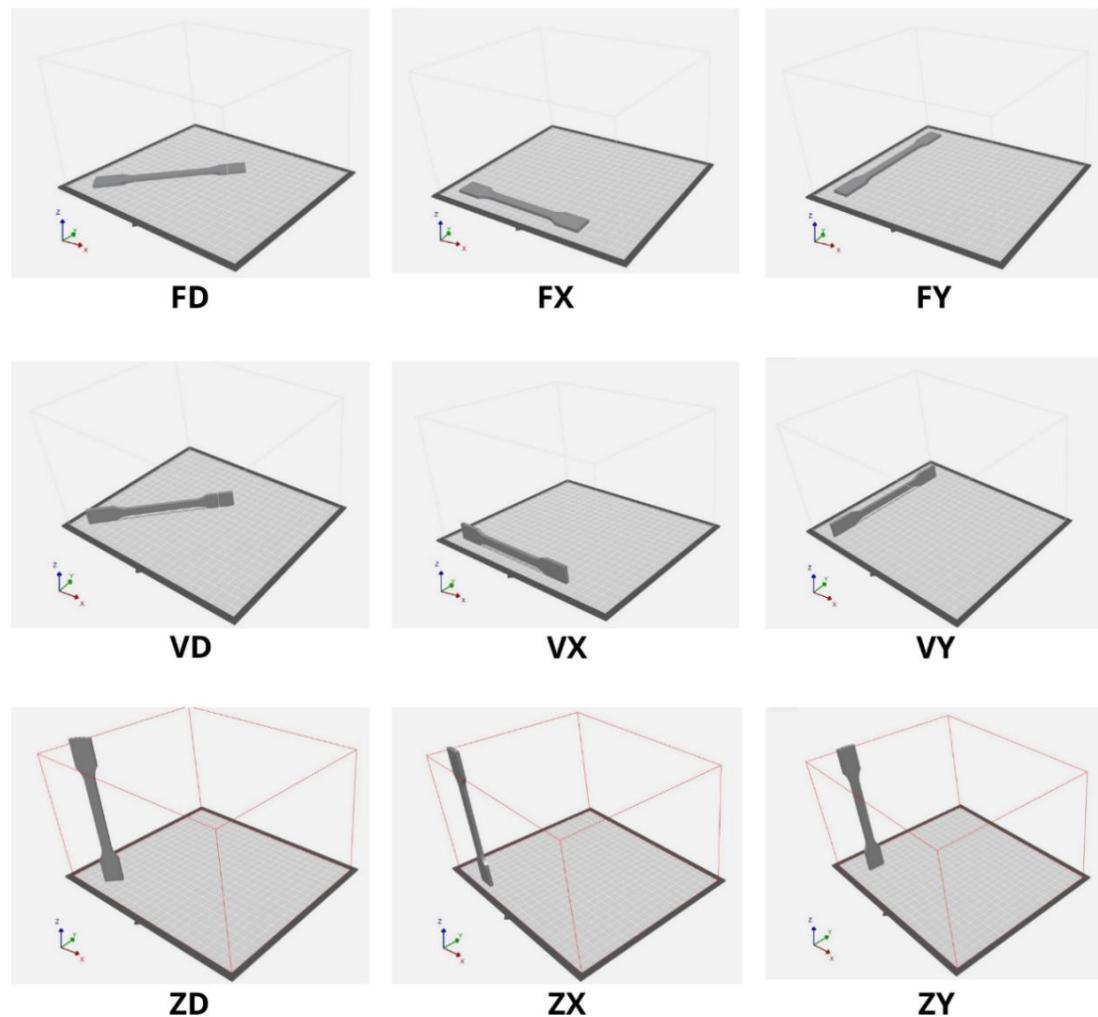


Figure 4.2 – The positioning and the given names of the nine different orientations chosen for producing the specimens by the two technologies

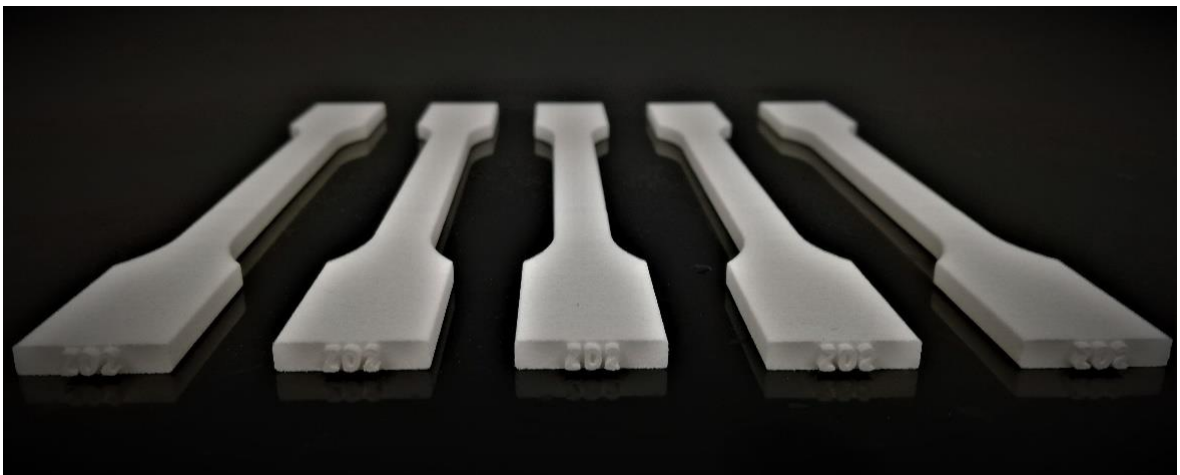
In figure 4.3 (c), the five-specimen produced in the ZD (axis align Z direction, and in 45 degrees in respect to the x-axis) are present. The ZD printed at the surface of each specimen in this direction is visible. The printed number “2” which is printed in all of the specimens printed with the SLS machine indicates the technology used to produce the specimen. In the case of a specimen printed by the MJF machine, there is a number “1” printed at the end of the name.



(a)



(b)



(c)

Figure 4.3 – (a) The specimens during the cleaning process, (b) All the SLS printed specimens after the post-processing stage, (c) The five specimens produced in the ZD orientation (axis align Z direction, and in 45 degrees in respect to the x-axis)

The output of each tensile test is a curve obtained by measuring the force and elongation through the sampling periods (figure 4.4). These values are recorded in the computer software of the tensile testing machine, and also there is the possibility of exporting the data in text format files.

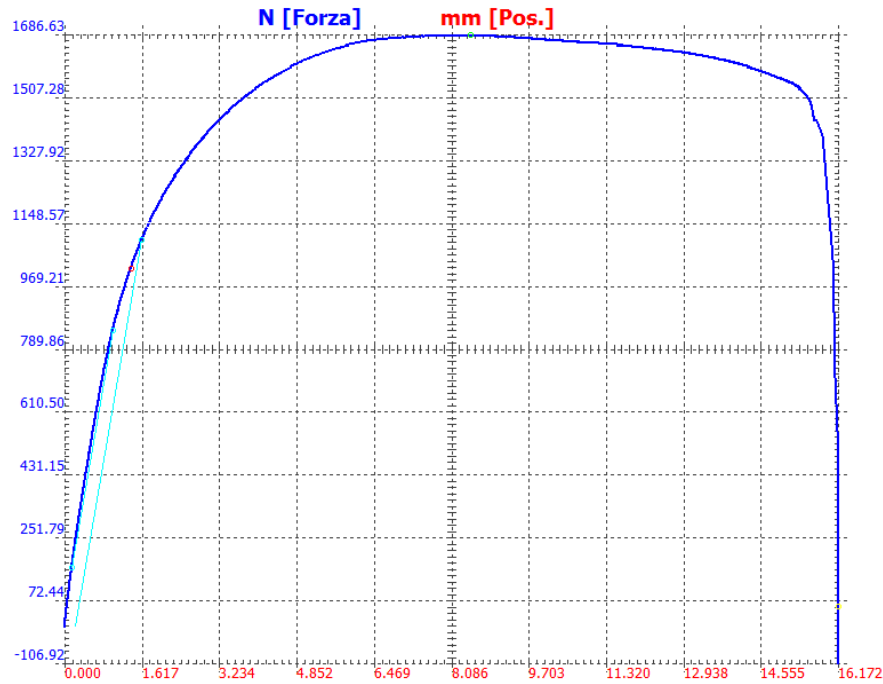


Figure 4.4 – The Force vs Elongation graph obtained by the tensile test machine for the specimen VXI

To have a clear view of the mechanical properties such as yield's stress value, Young's Modulus, etc. The force-elongation curve is not very useful. By dividing the force amount by the exact amount of the cross-section area measured for each specimen, the applied stress can be obtained.

The stress-strain curve is obtained for each specimen after importing the data received from the tensile test machine in MATLAB. Through simple coding in MATLAB, the yield points have been obtained. This point is an offset yield point (or proof stress) since the mechanical behavior of the material does not show an obvious yield point in the strain-stress diagram which is common for most nonferrous materials. In figure 4.5, the stress-strain diagram and the obtained yield point of the specimen No.2 of the VX orientation for the SLS technology are demonstrated.

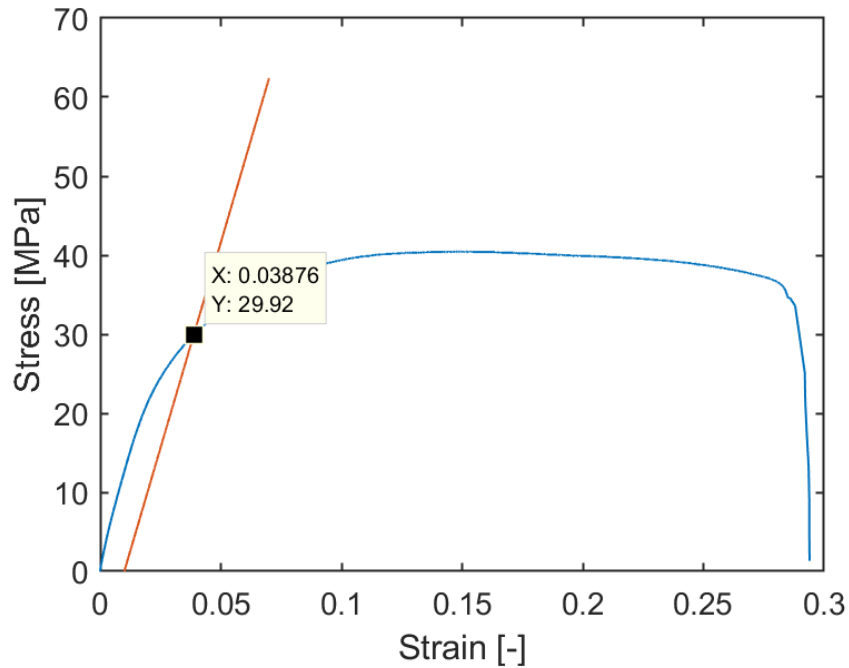


Figure 4.5 – The stress-strain diagram and the Yield Point for the specimen VX1, as the output of the MATLAB code

In this thesis six important mechanical properties obtained from the tensile tests are studied and compared for each technology; these six properties are as follows:

- 1- The Ultimate Tensile Strength [MPa] (σ_{UTS}); The maximum stress the material can withstand (based on the original cross-sectional area) [32].
- 2- The Yield Strength [MPa] (σ_Y); The maximum stress that can be applied without exceeding a specified value of permanent strain [32].
- 3- Elastic Modulus [Mpa]; Slope of the initial linear portion of the stress-strain diagram. The modulus of elasticity may also be characterized as the “stiffness” or ability of a material to resist under elastic deformation within the linear range [32].
- 4- Yield Point Elongation [%]; YPE is the strain of the specimen when it reaches the Yield point, expressed as a percentage [32].
- 5- Elongation at maximum force [%]; The strain of the specimen when it is under the maximum force applied during the test, expressed as a percentage [32].
- 6- Elongation at Break [%]; The strain at fracture in tension, expressed as a percentage = $\frac{(\text{final gage length} - \text{initial gage length})}{\text{initial gage length}} \times 100$. Percent elongation is a measure of ductility [32].

4.2. Results for Multi Jet Fusion technology

In this Chapter, all the experimental data for the Multi Jet Fusion technology are reported in specified tables for each mechanical property. Since there are 5 specimens produced for each orientation, the Standard Deviations are used to check the reliability of the results.

The ultimate tensile strength does not vary significantly for different orientations of the printed specimens (see figure 4.6). However, the ultimate tensile strength reported by the PA12 manufacturer in the datasheet (48 [Mpa]) is almost 20% more than the highest value recorded during the tensile tests in the IAM laboratory (40 [Mpa]). This difference in the values from the datasheet of the material and the experimental data is already anticipated since the specimens used for carrying out the tensile tests in this thesis are produced according to the real industry parameters. The powder used for producing the specimen was not all virgin powder, but the mixture of the virgin powder and the used powder, and this affects a lot the mechanical properties of the produced parts. Furthermore, several other parameters, such as the production speed, the designed layer thickness, etc. can have a big influence on the final results too.

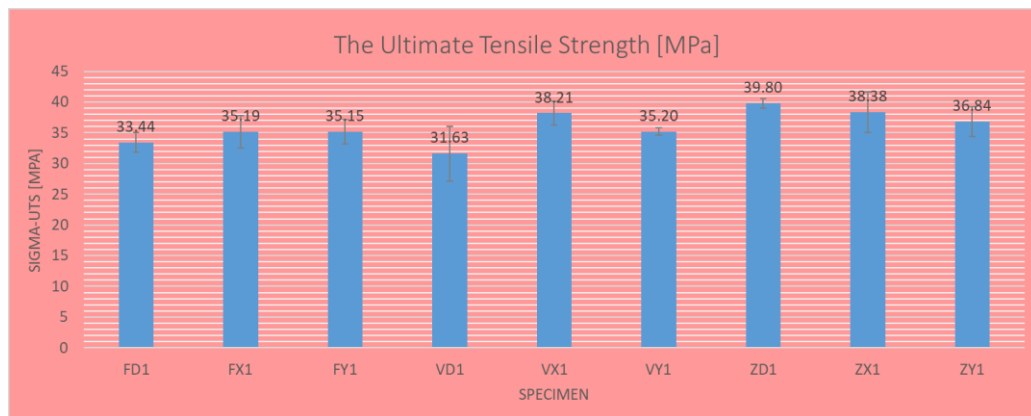


Figure 4.6 – The Ultimate Tensile Strength bar chart for the MJF specimens

The results for the yield strength values show the same situation as the ultimate tensile strength for the MJF specimens (see figure 4.7). The numbers are almost

in the same range, with the ZX orientation as the maximum mean value (almost 29.5 [Mpa]), and the VD as the minimum mean value of the 23.2 [Mpa].

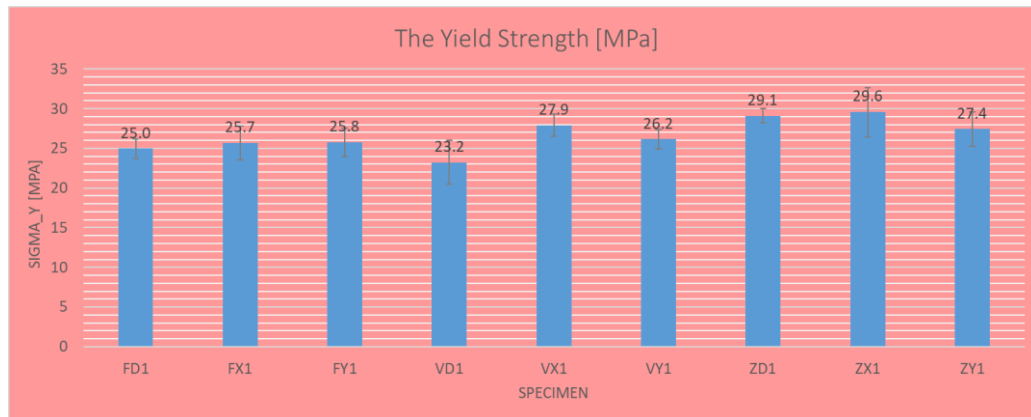


Figure 4.7 – The Yield Strength bar chart for the MJF specimens

Elastic Modulus values obtained differ much more for different orientations of the printing compared to the Sigma_{uts} & Sigma_y values. It is interesting to see that the mean Elastic Modulus values of the Z-axis specimens (ZD, ZX, and ZY) are even higher than the ones of the Flat and Vertical oriented specimens; however, this situation is reported as the same in the datasheet of the material (see table 2.7). The VD-oriented (Vertical and 45 degree oriented concerning the x-axis) specimens produced, show the value of 673 [Mpa] which is the lowest average value between all the produced orientations. The difference between the mean experimental Elastic Modulus values and the ones reported in the PA12 datasheet is a big number (e.g. almost 60% for the VD orientation), which can point out that using a mixed powder instead of the total virgin powder in MJF technology can affect the Elastic Modulus property much more than the strength properties of the produced parts.

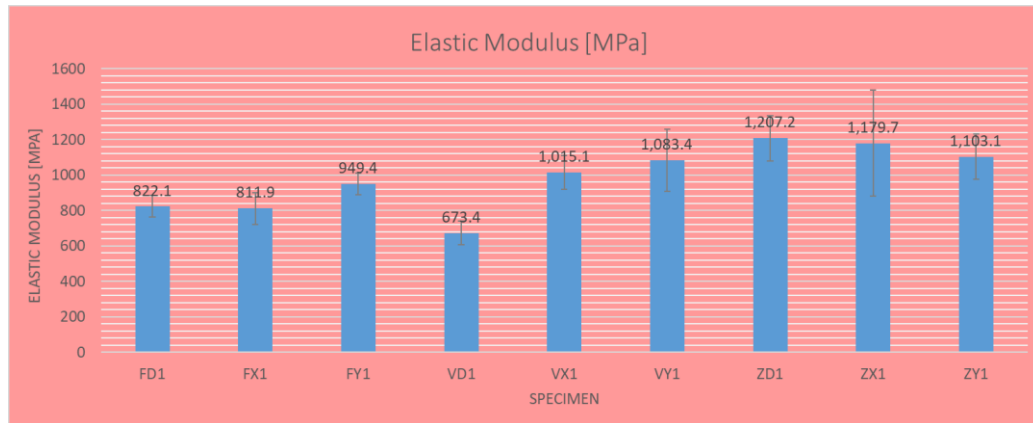


Figure 4.8 – The Elastic Modulus bar chart for the MJF specimens

The results for the MJF specimens Yield Point Elongation describes that all the specimens started to suffer from the permanent deformation after only 2% of the elongation of the specimens with a small variance for each printing orientation, and VD orientation shows the minimum Yield Point Elongation value (1.6 [%]).

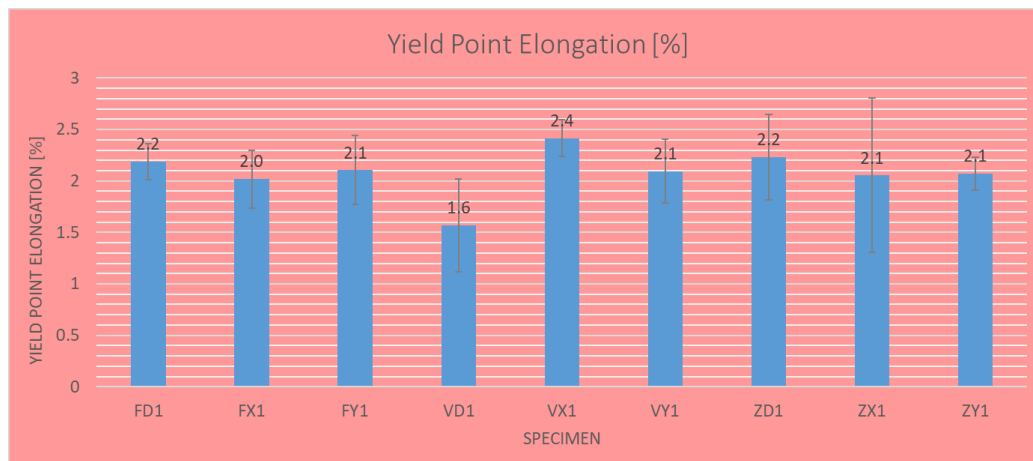


Figure 4.9 – The Yield Point Elongation bar chart for the MJF technology

Regarding the elongation at break (figure 4.10), it can be noticed that mean values obtained for the ZX orientation produced specimens are the least number, and it was anticipated by the logic of the 3d printing technology for the MJF, however, the interesting point is the difference of the values obtained for various orientations within the Flat and Vertical orientation specimen, somehow only the FX and VX are showing big difference compared to the other orientations, the values obtained for these two orientations are even higher than the ones reported in the material’s datasheet. The other point is the big amount of deviation in the

elongation at break values recorded for the 5 different specimens in the ZX direction. This is due to the sudden brittle rupture for some of the specimens produced in this orientation during the tensile tests.

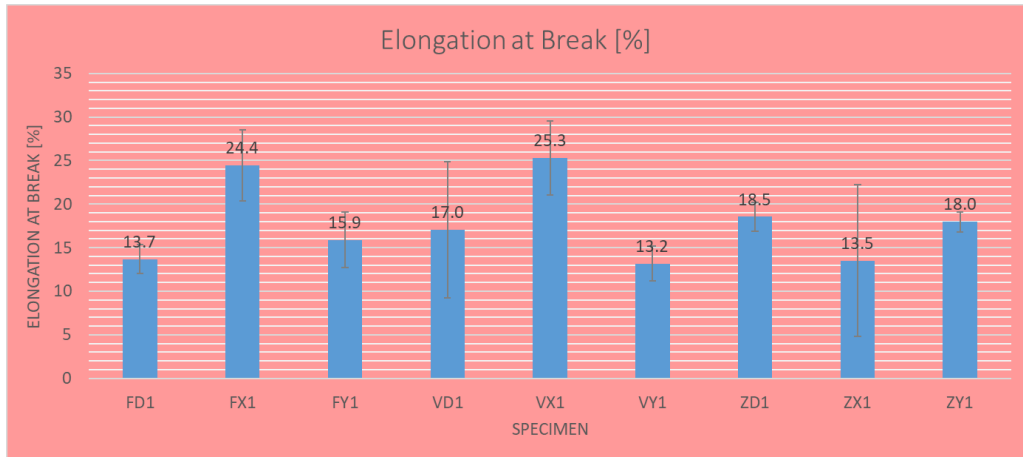


Figure 4.10 – The Elongation at Break bar chart for the MJF specimens

The difference between the Elongation at Maximum Force mean values and the Elongation at Break mean values are very different for each orientation of the printing. For the FD, FY, and VY, the difference is about 1%, but for the other specimens, there is a more deformation possibility after the necking is started.

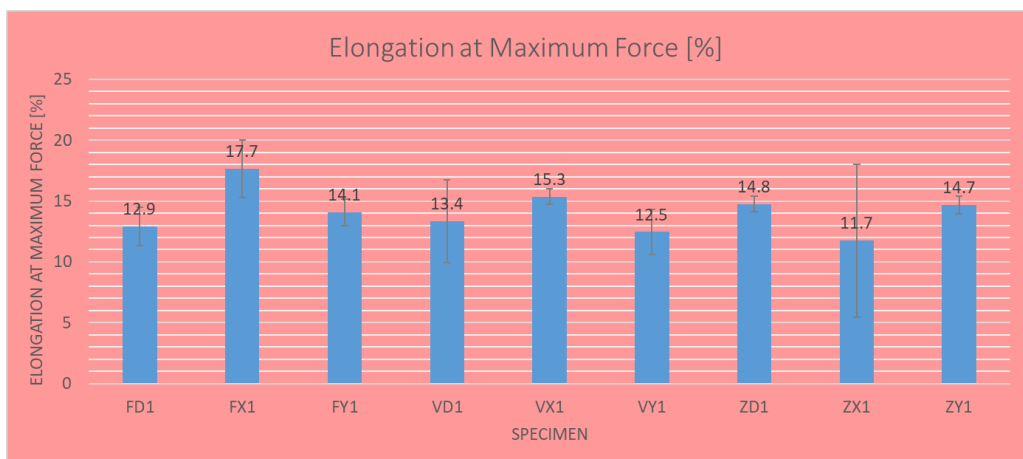


Figure 4.11 – The Elongation at Maximum Force bar chart for the MJF technology

4.3. Results for SLS Technology

Regarding the Ultimate Tensile Strength for the SLS specimens, the mean values obtained for different orientations, vary more than the ones of the MJF. The value reported in the datasheets of the PA2200 by the manufacturer (48 [Mpa]) is at least 20% higher than the ones recorded in the tensile tests; an amount of difference in the values gained in the laboratories and the values listed in the datasheets can be anticipated because of the same reasons mentioned before in the MJF section; which the most important one is the using of the mixed virgin and used powder for the production of the specimens. The least mean value of the ultimate tensile strength is for the ZY orientation (27.4 [Mpa]), and the highest mean value is for the FX orientation (40.1 [Mpa]) (see figure 4.12).

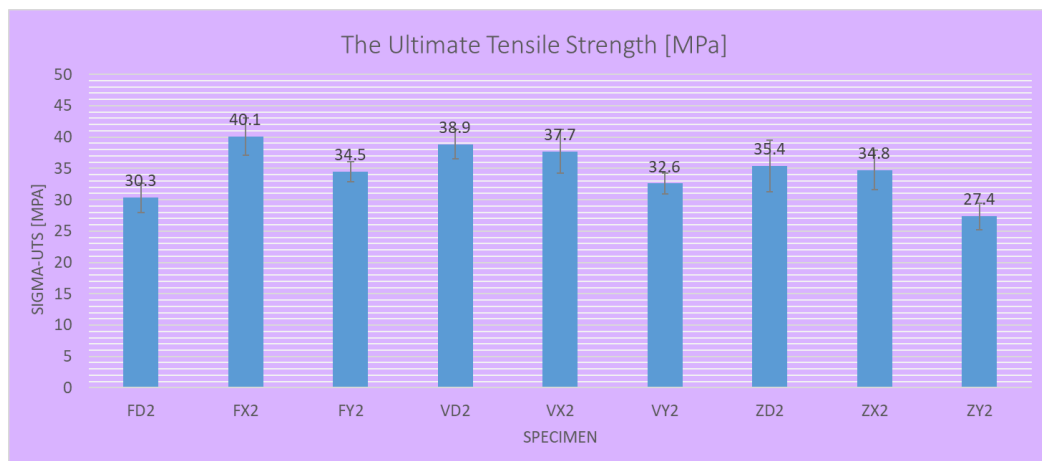


Figure 4.12 – The Ultimate Tensile Strength bar chart for the SLS specimens

The difference between the ultimate tensile strength and the yield strength in the SLS specimens produced by the SLS machine (see figure 4.13 & figure 4.12) is less than the ones produced by the HP MJF machine, and it means that the parts produced by the SLS technology can tolerate a higher amount of the stress before they start to have permanent deformations.

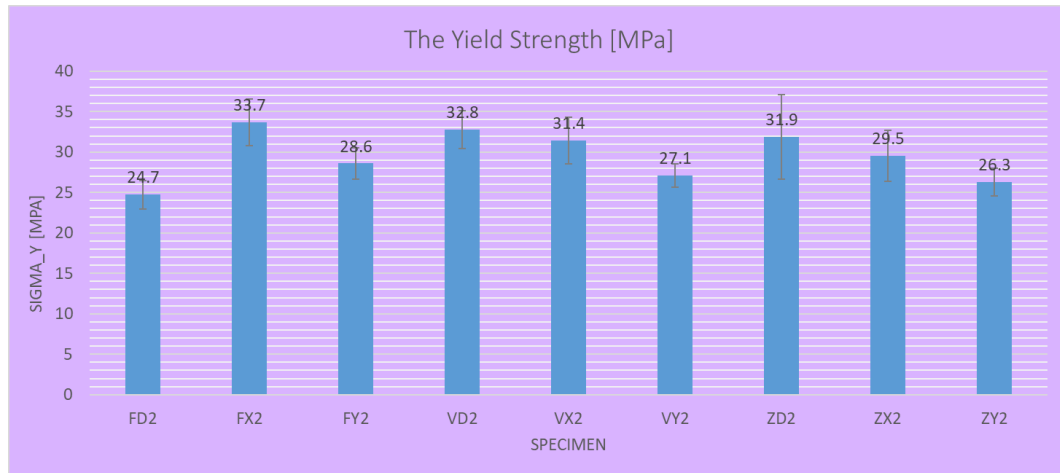


Figure 4.13 – The Yield Strength bar chart for the SLS specimens

The mean Elastic Modulus values of the SLS specimens are much closer to the ones reported by the manufacturer in the datasheets (1700 [Mpa]) in comparison with the MJF specimens; and in the ZX and FX orientations, it has the maximum values of about 1700 [Mpa] in ZX and FX printed orientations (see figure 4.14).

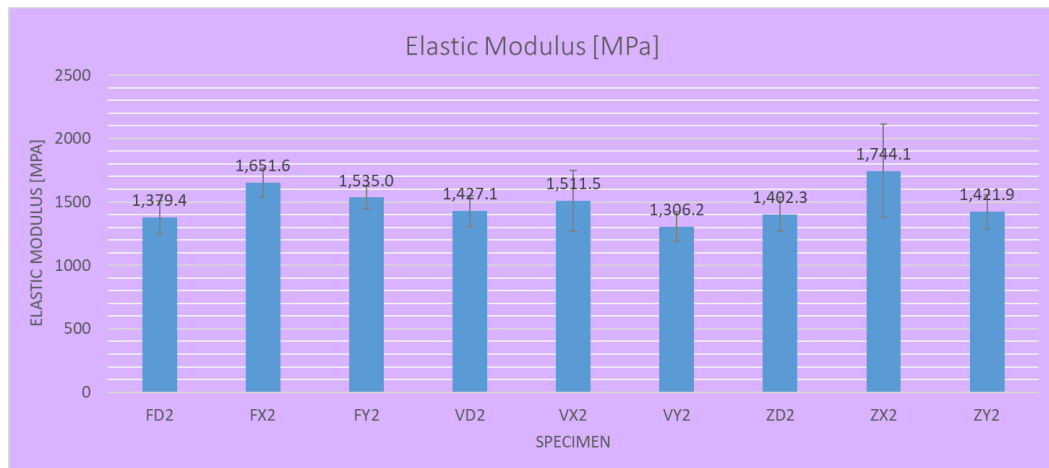


Figure 4.14 – The Elastic Modulus bar chart for the SLS specimens

The Yield Point Elongation mean values of the SLS specimens are very similar to the ones of the MJF specimens, and they are about 2%, which once again describes that the material will face a permanent deformation after it reaches a very low value of the elongation (less than 3% for all the orientations).

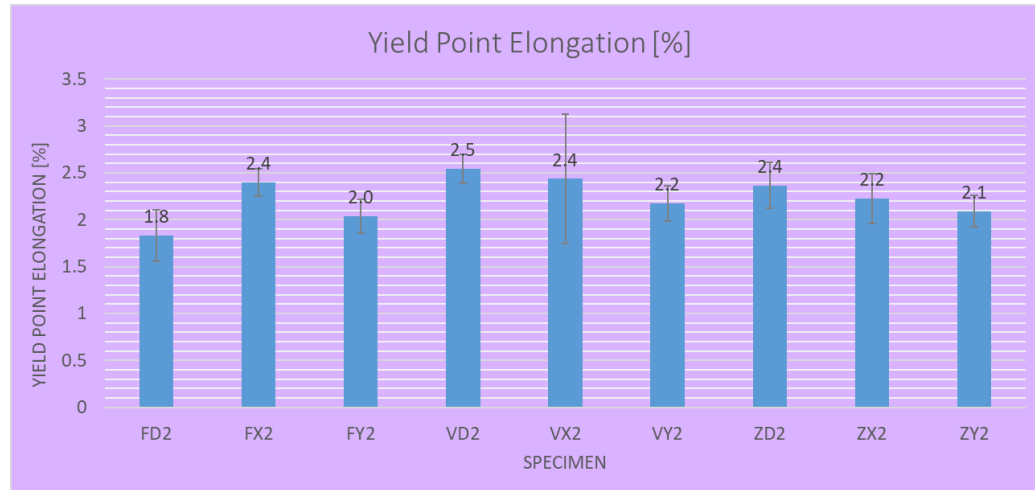


Figure 4.15 – The Yield Point Elongation bar chart for the SLS technology

The mean values for the elongation at break for all the z-axis orientations (ZD, ZX, and ZY) are significantly lower than the values obtained for the other orientations (see figure 4.16), in fact, in the other orientations, the mean values obtained for the elongation at break are even higher than the value reported in the datasheet of the material (24 [%]). The maximum mean value obtained for the elongation at break percentage in the SLS specimens is for the VY and FD orientations (30 [%]). The very low flexibility in the Z-axis specimens compared to the other specimens produced in the flat and the vertical orientations can be considered as a drawback for this technology.

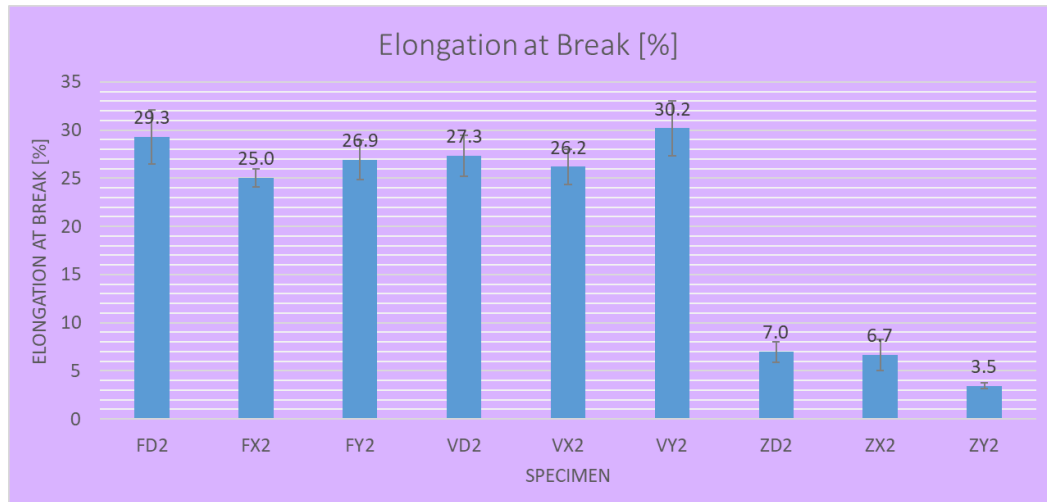


Figure 4.16 – The Elongation at Break bar chart for the MJF specimens

By comparing the results for the Elongation at Maximum Force mean values and the Elongation at Break mean values, it can be noticed that the mechanical behavior of the different SLS specimens differs significantly for the different specimen orientations. Only in Z-axis specimens, the two mean values are almost the same and very low, which means that these specimens will not experience necking in the tensile tests. On the contrary, in all the other printing orientation values, there is a big difference in the two elongations, and sometimes the Elongation at Break value of the specimen is two times of the Elongation at Maximum Force values (see figure 4.17 & figure 4.16).

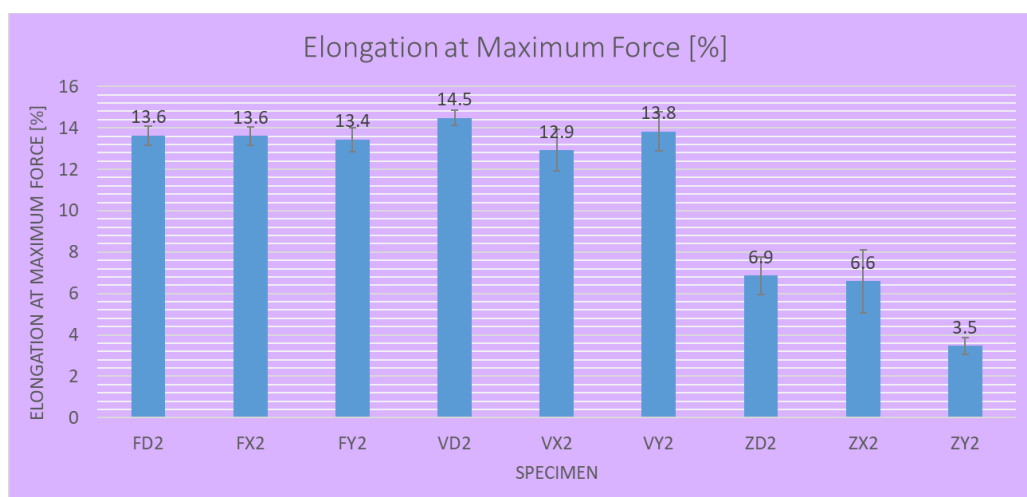


Figure 4.17 – The Elongation at Maximum Force bar chart for the SLS technology

4.4. Overall Comparison charts, MJF vs SLS

Regarding the Ultimate Tensile Strength, the values are almost the same for most of the orientations for the two technologies (see figure 4.18). The main difference is for the ZY orientation in which the mean value of the ultimate tensile strength for the MJF is higher than the value for the SLS by almost 10 [Mpa] which can be considered a big amount.

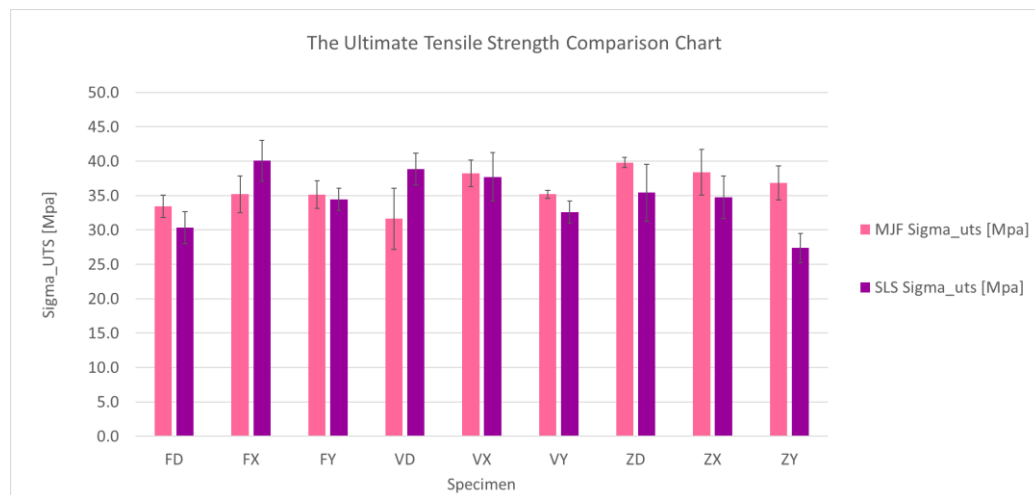


Figure 4.18 – The Ultimate Tensile Strength Comparison Chart for MJF & SLS

Regarding the Yield Strength, the values are different considerably only in FX and VD orientation (see Figure 4.19).

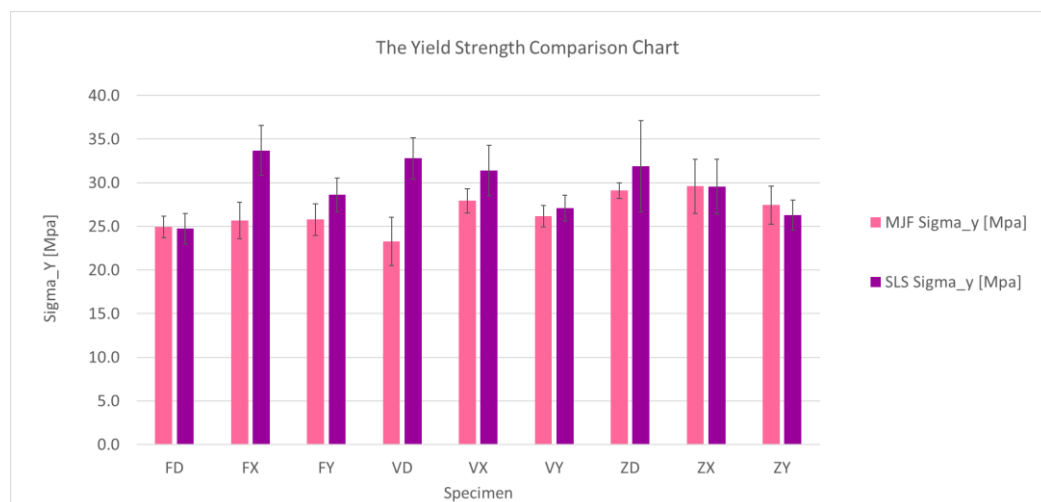


Figure 4.19 – The Yield Strength Comparison Chart for MJF & SLS

In the case of Elastic Modulus, the mean values are much more different for the two technologies than the values of the ultimate tensile strength and the yield strengths (Figure 4.20). It can be seen that the elastic modulus is much higher for the SLS specimens in all the produced orientations, especially in the flat (FD, FX, and FY) and vertical (VD, VX, and VY) ones.

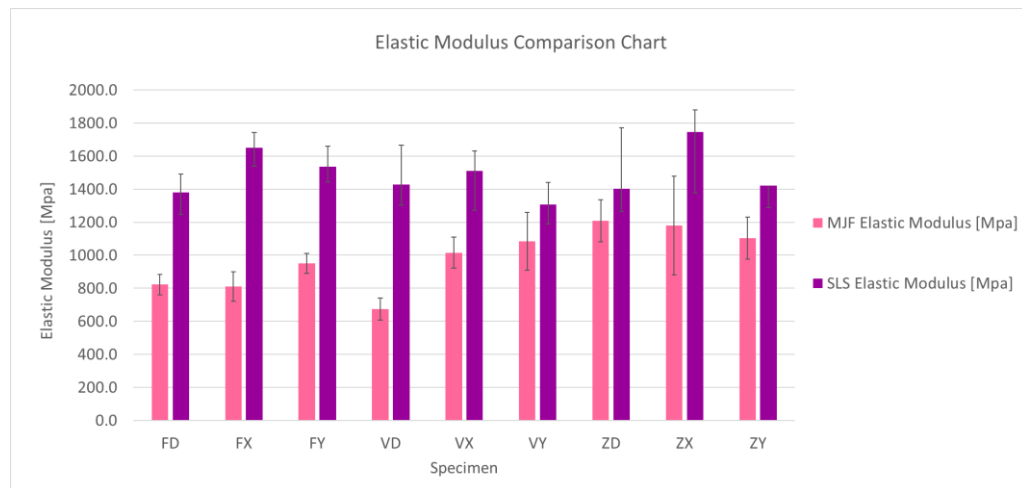


Figure 4.20 – Elastic Modulus Comparison Chart for MJF & SLS

As shown in figure 4.21, the Yield Point Elongation mean values for both of the technologies are around 2% which shows the lack of elastic deformation capacity.

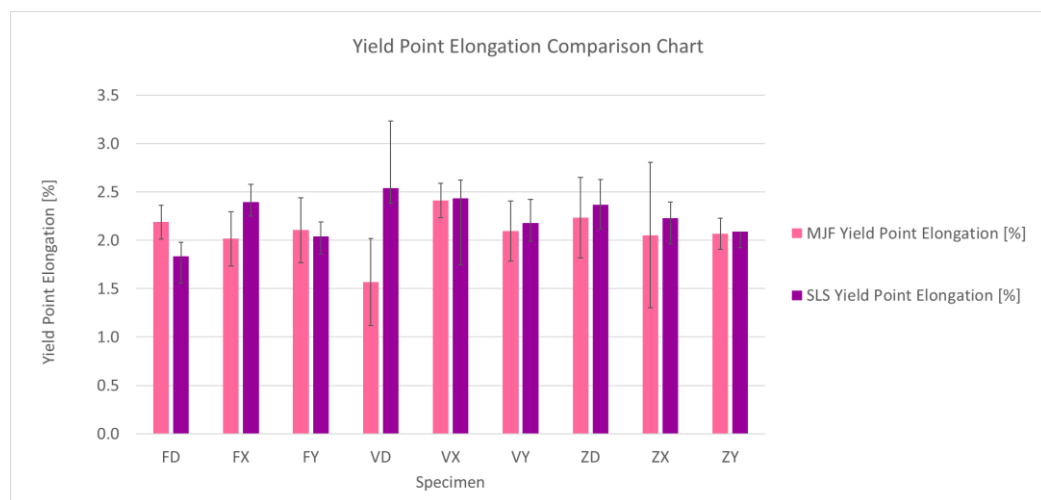


Figure 4.21 – Yield Point Elongation Comparison Chart for MJF & SLS

An interesting fact about the elongation at break comparison chart (figure 4.22) is that the values for the SLS specimens are much higher for all the Flat and Vertical orientations, but on the contrary, the values for the Z-axis oriented

specimen of the MJF specimens are much higher. These results about the maximum deformability of the two technologies in various production orientations can be a key factor to choose the production orientation for different designed parts after considering the direction of the mechanical loads they have to tolerate.

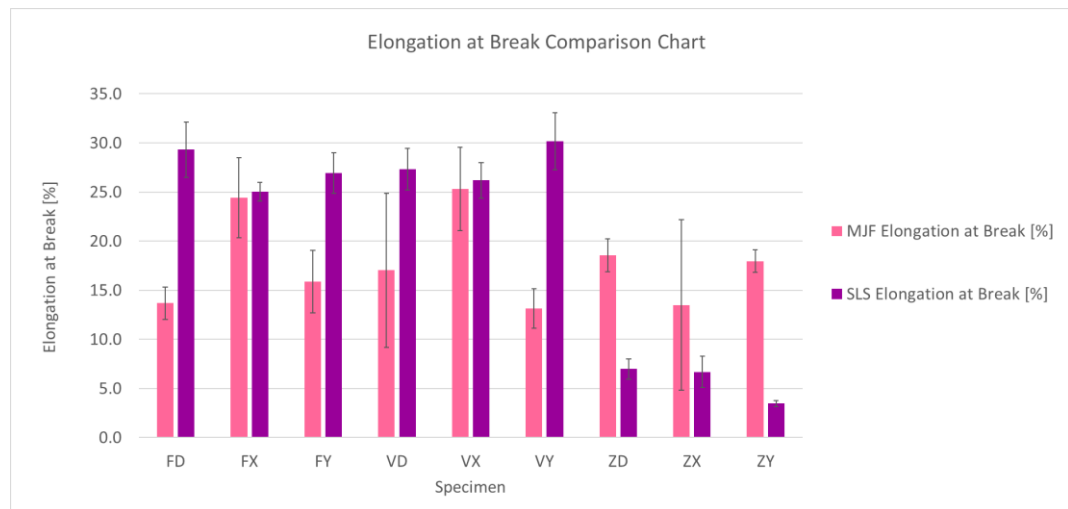


Figure 4.22 – Elongation at Break Comparison Chart for MJF & SLS

The chart for the elongation at the maximum force shows a big difference in the Z-oriented specimens between the two technologies. This difference in the values continues to increase until the rupture of the specimens as it can be seen in the previous (elongation at break [%]) comparison chart.

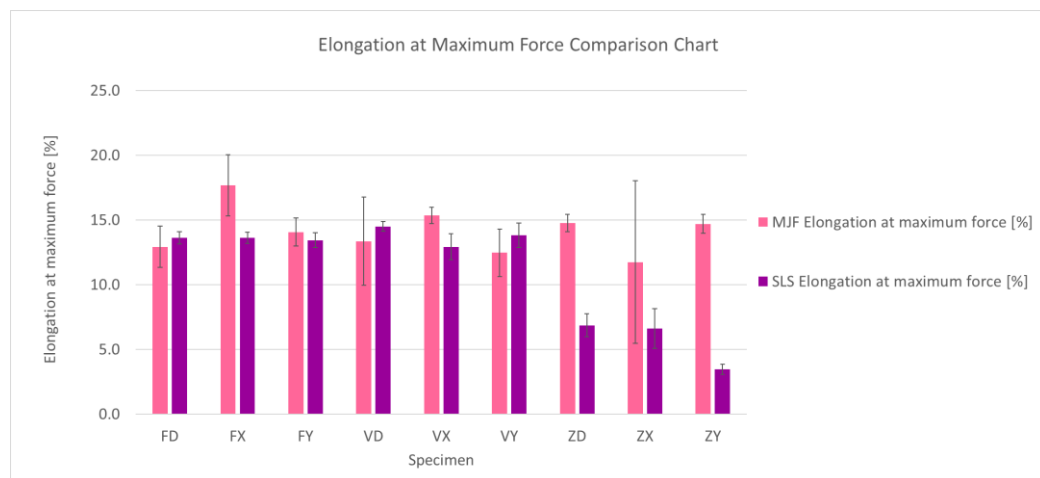


Figure 4.23 – Elongation at Maximum Force Comparison Chart for MJF & SLS

5. Conclusions

Additive manufacturing has been developed rapidly during the last decade, and there are many different technologies now in the 3D printing industries. However, when it comes to comparing these technologies, most of the times there are not dedicated standards and defined procedures to follow, and it makes the process of a good and acceptable comparison harder, especially since there are many parameters to set for each machine, from the printing speed to the layer thickness and some other important factors such as the cooling-down time after the production phase, and also the most important one, the type of material used, since there is usually more than one possible option for each machine, and they are designed for different purposes, and consequently with different mechanical properties.

However, in this thesis, the main purpose was to compare the technologies in the real industrial situation, since this thesis was done in collaboration with the FCA, which is a well-known multinational Automotive Corporation. Consequently, the parameters during the production phase especially were chosen as the ones that are set while producing the real parts in the FCA EMEA PD Additive Manufacturing Centre. The same situation applies for the powders too, and the mixed percentage of the virgin powder and the used powder were the same as the percentage of the real parts produced in this center.

Regarding the results obtained after 90 tensile tests carried out on the specimens for the two technologies, some similarities and some differences are noticeable in the comparison chart for each mechanical property reported in this study. According to the results, the main differences are related to the Elastic Modulus values, which for the SLS specimens, they are much higher than the values for the MJF specimens, and the Elongation at Break percentage, in which the SLS specimens show much more different behavior in different orientations of the production. This is very important in the part design process, since in this case for example the specimen produced in any of the Z-axis directions (ZD, ZX, and ZY) cannot be used in the condition which requires a fair amount of deformability. In this case, the material will show a sudden brittle fracture.

Besides the mechanical properties of the parts produced which was the main focus of this thesis, there are many other factors which are very important while choosing one of the two technologies for producing certain parts, and sometimes even more important than the mechanical properties, such as the powder price, the speed of the production, and also the price of the machine itself.

A. List of Tables

Table 1.1 – Classification of Powder bed fusion/additive manufacturing technology

Table 1.2 – Laser sintering process parameters

Table 1.3 – Results for EOS Polyamide 12 (PA 2200)

Table 1.4 – Results for EOS Polyamide 11 (PA 1102 Black)

Table 1.5 – HP 3D High Reusability PA 12 characteristics

Table 1.6 – Results for HP 3D High Reusability PA 12

Table 1.7 – HP 3D High Reusability PA 11 characteristics

Table 1.8 – Results for HP 3D High Reusability PA 11

Table 1.9 – HP 3D High Reusability PA 12 Glass Beads characteristics

Table 1.10 – Results for HP 3D High Reusability PA 12 Glass Beads

Table 1.11 – HP 3D High Reusability PP characteristics

Table 1.12 – Results for HP 3D High Reusability PP

Table 2.1 – Technical Data for FORMIGA P 110 Velocis AM machine

Table 2.2 – EOS SLS Polymer Materials portfolio selection guide

Table 2.3 – HP Jet Fusion 4200 3D printing and cooling time

Table 2.4 – HP Jet Fusion 4200 3D printing speed options considering the powder type

Table 2.5 – HP Jet Fusion 4200 3D natural and fast cooling processes time

Table 2.6 – HP 3D Printing materials portfolio selection guide

Table 2.7 – HP MJF PA 12 material datasheet

Table 2.8 – EOS PA 12 (PA 2200) material datasheet

Table 3.1 – The details of the geometry of the specimen (ISO 3167 type 1A standard)

B. List of Figures

Figure 1.1 – The 3d printing technology schematic steps

Figure 1.2 – Global Additive Manufacturing segmentation

Figure 1.3 – Using Additive Manufacturing parts in the industries

Figure 1.4 – The Additive Manufacturing Market size anticipation

Figure 1.5 – The revenue generation anticipation for the future of Additive manufacturing (2015-2025)

Figure 1.6 – Schematic of the printing process for a PBF technology (SLS in this case)

Figure 1.7 – Schematic illustrating the ability of polymer powder bed fusion to produce parts with overhangs and unsupported islands without support structures (left) compared with other AM processes, for example, fused deposition modeling (right), in which these structures must be supported during the build process.

Figure 1.8 – A typical laser sintering build set-up consisting of multiple individual parts. Because no support structures are required, parts can be placed freely in the entire build volume without being connected to the part below.

Figure 1.9 – Schematic of a simplified laser sintering technology

Figure 1.10 – Parallel-line scan mode in the same and alternate directions.

Figure 1.11 – Schematic of HP Multi Jet Fusion synchronous printing architecture

Figure 1.12 – Schematic of HP Multi Jet Fusion printing process, cross-sectional views (for each specific HP MJF machine model, some steps may differ in the process)

Figure 1.13 – Pixel, binary voxel, and HP Multi Jet Fusion voxels

Figure 1.14 – Sample parts made by HP Multi Jet Fusion technology

Figure 2.1 – SLS 3D Printer FORMIGA P 110 Velocis

Figure 2.2 – Compatible materials with the SLS 3d printer FORMIGA P 110 Velocis

Figure 2.3 – HP Jet Fusion 4200 3D Printing Solution

Figure 2.4 – Schematics of HP Jet Fusion 4200 printing procedure

Figure 2.5 – HP SmartStream 3D Build Manager user interface 1- Progress bar showing the progress of the build, 2- Job name, 3- Job cross-section image showing the slice currently printing

Figure 2.6 – HP Jet Fusion 4200 printheads 1- Rear printhead, 2- Middle printhead, 3- Front printhead

Figure 2.7 – HP Jet Fusion 4200 cartridges

Figure 2.8 – HP Jet Fusion 4200 minimum printable features in planes X, Y, and Z

Figure 2.9 – HP Jet Fusion 4200 processing station

Figure 2.10 – HP Jet Fusion 4200 processing station reusable material collector

Figure 2.11 – Morphology of PA powders: (a) PA12_ref, (b) PA12_EOS, and (c) PA12_MJF (scale bar: 200 μm)

Figure 3.1 – Schematic diagram of Tensile Testing Machine

Figure 3.2 – Load-deformation and the obtained Stress-strain diagram for 3 Aluminum alloy specimens with different geometry (2017-T451 Aluminum Alloy)

Figure 3.3 – The stress-strain curve of a material with the visible Yield Point (left), and without a visible Yield Point (right)

Figure 3.4 – Stress-strain curves for a polymer at T below and above the glass temperature

Figure 3.5 – The drawing of the specimen according to the ISO 3167 type 1A standard

Figure 3.6 – The drawing of the used specimen in the thesis (ISO 3167 type 1A) in CATIA V5

Figure 3.7 – The improvement of the “.stl” format files after increasing the edge quality of the design in CATIA V5, the surface design is smoother from left to right

Figure 4.1 – The arrangement of the 45 specimens in the build volume of the HP Jet Fusion 4200 (380 x 284 x 380 mm), according to the designed orientations. Isometric-view (left) and bottom view (right)

Figure 4.2 – The positioning and the given names of the nine different orientations chosen for producing the specimens by the two technologies

Figure 4.3 – 1- The specimens during the cleaning process, 2- All the SLS printed specimens after the post-processing stage, 3- The five specimens produced in the ZD orientation (axis align Z direction, and in 45 degrees in respect to the x-axis)

Figure 4.4 – The Force vs Elongation graph obtained by the tensile test machine for the specimen VX1

Figure 4.5 – The stress-strain diagram and the Yield Point for the specimen VX1, as the output of the MATLAB code

Figure 4.6 – The Ultimate Tensile Strength bar chart for the MJF specimens

Figure 4.7 – The Yield Strength bar chart for the MJF specimens

Figure 4.8 – The Elastic Modulus bar chart for the MJF specimens

Figure 4.9 – The Yield Point Elongation bar chart for the MJF technology

Figure 4.10 – The Elongation at Break bar chart for the MJF specimens

Figure 4.11 – The Elongation at Maximum Force bar chart for the MJF technology

Figure 4.12 – The Ultimate Tensile Strength bar chart for the SLS specimens

Figure 4.13 – The Yield Strength bar chart for the SLS specimens

Figure 4.14 – The Elastic Modulus bar chart for the SLS specimens

Figure 4.15 – The Yield Point Elongation bar chart for the SLS technology

Figure 4.16 – The Elongation at Break bar chart for the MJF specimens

Figure 4.17 – The Elongation at Maximum Force bar chart for the SLS technology

Figure 4.18 – The Ultimate Tensile Strength Comparison Chart for MJF & SLS

Figure 4.19 – The Yield Strength Comparison Chart for MJF & SLS

Figure 4.20 – Elastic Modulus Comparison Chart for MJF & SLS

Figure 4.21 – Yield Point Elongation Comparison Chart for MJF & SLS

Figure 4.22 – Elongation at Break Comparison Chart for MJF & SLS

Figure 4.23 – Elongation at Maximum Force Comparison Chart for MJF & SLS

C. Abbreviations

AM – Additive Manufacturing

CAD – Computer-Aided Design

PBF – Powder Bed Fusion

SLS – Selective Laser Sintering

MJF – Multi Jet Fusion

STL – Standard Triangulation Language

FCA – Fiat Chrysler Automobiles

IAM – Integrated Additive Manufacturing

FCA – Fiat Chrysler Automobiles

PoliTo – Politecnico di Torino

EOS – Electro Optical Systems Ltd

ISO – International Organization for Standardization

D. Bibliography

- [1] "3D printing scales up," *The Economist*, 5 September 2013.
- [2] J. Excell, "The rise of additive manufacturing," *The Engineer (Retrieved)*, 30 October 2013.
- [3] "Learning Course: Additive Manufacturing – Additive Fertigung," TMG (TECHNOLOGY MANAGEMENT GRUPPE), [Online]. Available: tmg-muenchen.de.
- [4] "Most used 3D printing technologies 2017–2018 | Statista," Statista (Retrieved), 2 December 2018. [Online]. Available: <https://www.statista.com/statistics/560304/worldwide-survey-3d-printing-top-technologies/>.
- [5] "ADDITIVE MANUFACTURING," GE Additive, [Online]. Available: <https://www.ge.com/additive/additive-manufacturing>.
- [6] T. Campbell, C. Williams, O. Ivanova and B. Garrett, "Could 3D Printing Change the World? Technologies, Potential, and Implications of Additive Manufacturing," 2011.
- [7] D. Dimitrov, N. d. Beer, P. Hugo and K. Schreve, "10.08 - Three Dimensional Printing," in *Comprehensive Materials Processing*, Stellenbosch University, South Africa, Elsevier B.V., 2014, pp. Pages 217-250.
- [8] A. Agarwal and S. Khavnekar, "Additive Manufacturing — The Next Industrial Revolution?," 31 August 2017. [Online]. Available: <https://www.aranca.com/knowledge-library/blogs-and-opinions/business-research/additive-manufacturing-the-next-industrial-revolution>.
- [9] "clearwater international," January 2018. [Online]. Available: <https://www.clearwaterinternational.com/assets/pdfs/Additive-manufacturing-clearview.pdf>.
- [10] J. Mericle, "ExOne licenses new 3D printing method with high-value production in mind," *Pittsburgh Business Times*, 2019.
- [11] D. Sher, "The global additive manufacturing market 2018 is worth \$9.3 billion," 14 December 2018. [Online]. Available: <https://www.3dprintingmedia.network/the-global-additive-manufacturing-market-2018-is-worth-9-3-billion/>.
- [12] "Global Additive Manufacturing Market, Forecast," Frost & Sullivan's Global 360° Research Team, 2016.
- [13] R. Goodridge and S. Ziegelmeier, "Powder bed fusion of polymers," in *Laser Additive Manufacturing*, Woodhead Publishing Series in Electronic and Optical Materials, 2017, pp. 181-204.
- [14] "The Powder Bed Fusion process," Prima Additive, [Online]. Available: <https://www.primaadditive.com/the-powder-bed-fusion-process/>.
- [15] R. Velu, F. Raspall and S. Singamneni, "Chapter 8 - 3D printing technologies and composite materials for structural applications," in *Green Composites for Automotive Applications*, Woodhead Publishing Series in Composites Science and Engineering, 2019, pp. 171-196.

- [16] S. Kumar, "10.05 Selective Laser Sintering/Melting (University of Michigan – Shanghai Jiao Tong University Joint Institute, Shanghai, China)," 2014 Elsevier Ltd., pp. 94-131.
- [17] "EOS 3D Printing, Materials Plastics for AM, SLS Materials and Processes," EOS, [Online]. Available: <https://www.eos.info/en/additive-manufacturing/3d-printing-plastic/sls-polymer-materials>.
- [18] "Polyamide 12 for 3D Printing," EOS, [Online]. Available: <https://www.eos.info/en/additive-manufacturing/3d-printing-plastic/sls-polymer-materials/polyamide-pa-12-alumide>.
- [19] "polyamide 11, Nylon for 3D Printing," EOS, [Online]. Available: <https://www.eos.info/en/additive-manufacturing/3d-printing-plastic/sls-polymer-materials/pa-11-nylon-abs-pa6>.
- [20] "HP Jet Fusion 4200 3D Printing Solution User Guide Edition 6, HP Development Company, L.P.," [Online]. Available: <https://support.hp.com/us-en/product/hp-jet-fusion-3d-4200-printer/11461058/manuals>.
- [21] "HP Multi Jet Fusion technology Technical white paper, HP Development Company, L.P.," [Online]. Available: <https://enable.hp.com/us-en-3dprint-wp-technical>.
- [22] "HP 3D Printing materials, HP Development Company, L.P.," [Online]. Available: <https://www8.hp.com/ie/en/printers/3d-printers/materials.html>.
- [23] "HP 3D Printing materials for the HP Jet Fusion 4200 3D Printing Solution_ White paper, HP Development Company, L.P.," [Online]. Available: <https://h20195.www2.hp.com/V2/getpdf.aspx/4AA7-7085ENW.pdf>.
- [24] "HP 3D Printing materials for the HP Jet Fusion 5200 Series 3D Printing Solution_ White paper, HP Development Company, L.P.," [Online]. Available: <https://h20195.www2.hp.com/V2/getpdf.aspx/4AA7-7084ENW.pdf>.
- [25] "HP 3D Printing materials, HP Development Company, L.P.," [Online]. Available: <https://www8.hp.com/us/en/printers/3d-printers/materials.html?m802=1&tab=2>.
- [26] EOS, "FORMIGA P 110 Velocis," [Online]. Available: <https://www.eos.info/en/additive-manufacturing/3d-printing-plastic/eos-polymer-systems/formiga-p-110-velocis>.
- [27] EOS, "EOS Materials Plastic Technical Data," [Online]. Available: https://www.eos.info/03_system-related-assets/material-related-contents/material_pdf/eos_p_materials-system_compatibility_overview_en_web.pdf.
- [28] "HP - 3D Printer - Jet Fusion 3D 4200 Printing Solution," [Online]. Available: <https://www.dksh.com/global-en/products/mac/hp-3dprinter-jetfusion-3d-4200>.
- [29] "HP Jet Fusion 4200 3D Printing Solution Brochure," [Online]. Available: <https://www8.hp.com/h20195/v2/GetDocument.aspx?docname=4AA6-4892ENA>.
- [30] "PA 12 (MJF)," Materialise, [Online]. Available: <https://www.materialise.com/en/manufacturing/materials/pa-12-mjf>.
- [31] "PA 2200 Material data sheet, GmbH, EOS," [Online]. Available: www.eos.info.

- [32] "Stress – Strain Relationships (Mechanical Design in Optical Engineering_ University of Arizona)," [Online]. Available: https://wp.optics.arizona.edu/optomech/wp-content/uploads/sites/53/2016/10/OPTI_222_W4.pdf.
- [33] "Universal Testing Machines - Tensile Tester," [Online]. Available: <https://www.torontech.com/servo-hydraulic-universal-testing-machine>.
- [34] "Chapter 6, Beyond elasticity: plasticity, yielding and ductility, Lecture notes version 4," TU Delft OpenCourseWare, 2011.
- [35] ISO, "Plastic - Multipurpose test specimens (International Standard ISO 3167 Forth edition preview version)," [Online]. Available: <https://www.sis.se/api/document/preview/899511/>.

E. Acknowledgments

This work was done in a collaboration of the Fiat Chrysler Automobiles EMEA PD Additive Manufacturing Centre with Politecnico di Torino Integrated Additive Manufacturing (IAM@PoliTO) Center. First, I would like to express my gratitude to my thesis supervisors, Prof. Luca Iuliano and Prof. Flaviana Calignano, for their availability and fast responses whenever I needed guidance through all the stages of the thesis.

Moreover, I would like to express my special thanks to Eng. Roberta Sampieri, Additive Manufacturing & Innovation Manager in FCA, who made the collaboration and the accessibility to the very advanced FCA Additive Manufacturing Centre possible, and also Eng. Stefano Paradiso in the FCA who helped during the production phase of the specimens.

I am grateful for the assistance given by Federico Giuffrida and Marco Viccica, the research fellows in the IAM center at the time.

I wish to express my appreciation to Claudio Riccardino, Manufacturing Senior Specialist in CNH Industrial AG Tractor Segment, who at the time of the thesis was my direct manager during my internship period in CNH industrial, and who made it possible for me to continue working on the thesis in some working days.

I would like to express my very great appreciation to my friends and my classmates who helped me during my master's degree studies, particularly Ali Ayati, Ehsan Kharrazi, Farid Jafari, and Roberto Culiarsi.

I should like to express my gratitude to all the professors and staff in Politecnico di Torino, who made my journey as an international student in Italy memorable.

Finally, I want to thank my parents and my entire family who without all their help and support I would not reach my goals in my life.